NORTHWESTERN UNIVERSITY

Integration of Synaptic Excitation and Inhibition in the Cerebellar Nuclei

A DISSERTATION

SUBMITTED TO THE GRADUATE SCHOOL

INPARTIAL FULFILLMENT OF THE REQUIREMENTS

For the degree

DOCTOR OF PHILOSOPHY

Field of Neuroscience

By

Yeechan Wu

EVANSTON, ILLINOIS

December 2017

Abstract

Large projection neurons of the cerebellar nuclei (CbN cells), whose activity generates movement, are inhibited by Purkinje cells and excited by mossy fibers. The high convergence, firing rates, and strength of Purkinje inputs predict powerful suppression of CbN cell spiking, raising the question of what activity patterns favor excitation over inhibition. Recording from CbN cells at near-physiological temperatures in cerebellar slices from weanling mice, we measured the amplitude, kinetics, voltage-dependence, and short-term plasticity of mossy fiber-mediated EPSCs. Unitary EPSCs were small and brief (AMPAR, ~1 nS, ~1 ms; NMDAR ~0.6 nS, ~7 ms) and depressed moderately. Using these experimentally measured parameters, we applied combinations of excitation and inhibition to CbN cells with dynamic clamp. Because Purkinje cells can fire coincident simple spikes during cerebellar behaviors, we varied the proportion (0-20 of 40) and precision (0-4 ms jitter) of synchrony of inhibitory inputs, along with the rates (0-100 spikes/s) and number (0-800) of excitatory inputs. Even with inhibition constant, when inhibitory synchrony was higher, excitation increased CbN cell firing rates more effectively. Partial inhibitory synchrony also dictated CbN cell spike timing, even with physiological rates of excitation. These effects were present with ≥10 inhibitory inputs active within 2-4 ms of each other. Conversely, spiking was most effectively suppressed when inhibition was maximally asynchronous. Thus, the rate and relative timing of Purkinje-mediated inhibition set the rate and timing of cerebellar output. The results suggest that increased coherence of Purkinje cell activity can facilitate mossy-fiber-driven spiking by CbN cells, in turn driving movements.

Acknowledgements

First, I would like to thank my mentor, Dr. Indira Raman. Indira, I feel so grateful and lucky to be able to work in your lab. You have been so patient to me especially when I use English to discuss experiments with you; I think I would not have felt so comfortable and confident speaking in English if my first mentor was not you. Furthermore, you always teach me to look up the data optimistically. There are so many times when I thought the data is not what I expected, but you taught me the data is the data, we just need to find another way to explain it. In your lab, I have learned not only the experimental techniques, but more importantly the way and attitude to do science; that is integrity and enthusiasm. Finally, you always care about me and my life and makes me feel safe and warm in this country especially when I am without my family. Thank you very much!

Next, I would like to thank my lab partner: Dr. Abigail Person, Dr. Jason Bant, Dr. Amanda Lewis, Dr. Marion Najac, Dr. Rashmi Sarnaik, Dr. Audrey Mercer, Dr. Chris Vaaga, Tom Harmon, Spencer Brown, Hayley White, Uri Magaram, and Taylor Jefferson. You always provide super helpful advices and inputs in the lab meeting; the way of meeting held in this lab is so enjoyable and is my precious experience in my Ph.D. life. It would not be so insightful and fun without your participation. You also help me so much not only for troubleshooting problems but also makes me so happy during my research. Thank you!

To my committee members: Dr. Daniel Dombeck, Dr. Marco Martina and Dr. David McLean, thank you for giving me so many feedbacks during the committee meeting. I really like the discussion type meeting, it makes me feel so relax and so eager to discuss my data and my thoughts with you. You have also been so kind to carefully explain what you have concerned about this project, and it makes me think this whole project more thoroughly. Thank you so much!

Finally, I would like to thank my family and my friends for all the support. When I felt sad, you cheered me up; when I felt successful, you were happy for me. Ph.D. is a very long period, and I would not have gone through it without your support. Although I never said anything about all the supports you have given to me, but in my mind, you are very important to me. To Mom, Dad, and I-Hsuan, thank you so much for supporting me for such a long time. Thank you for being so considered for helping me when I needed it and giving me space when I had to concentrate on working. Thank you so much!!

Table of contents

List of Figures

Chapter 1: Introduction

The goal of this study is to examine the integration of synaptic inputs in the mouse cerebellum. Specifically, cellular electrophysiological recording was performed on large, putative glutamatergic cerebellar nuclear cells to record action potential firing, while synaptic excitation and inhibition from mossy fibers and Purkinje cells were stimulated either with electrical stimulation or applied by computer simulated conductance. As the cerebellar output projection neurons, the activity of the large nuclear cells directly represents the final cerebellar signal and is modulated by many inputs from peripheral, cerebral cortex, and cerebellar cortex. In general, most of these synaptic inputs can be further divided into extra-cerebellar excitatory inputs from peripheral and cerebral cortex as mossy fibers and intra-cerebellar inhibitory inputs from cerebellar cortical Purkinje cells; these two inputs along with the intrinsic excitability of nuclear cells shape the final activity of nuclear cells. In particular, this study focused on the interaction between mossy fibers and Purkinje cell synchrony, which is one of the population firing patterns that has been discovered during cerebellar behavior. Understanding synaptic integration by nuclear cells requires the knowledge of the intrinsic properties of nuclear cells, firing properties and synaptic properties of both mossy fibers and Purkinje cells, as well as the extent of Purkinje cell synchrony. This introduction will provide the background information for aspects of these topics that are the most pertinent to the present study.

1.1 Function and anatomy of the cerebellar nuclei

The cerebellar nuclei are the sole outputs of the non-vestibular cerebellum; the activity of the cerebellar nuclear cells has already been found to be involved in many aspects of motor related physiology. For example, in motor control, extracellular recording of large, putative glutamatergic nuclear projection neurons (CbN cells) from monkeys showed correlation of firing rates to fore limb and hind limb movements (Thach, 1968; van Kan et al., 1993b); recording from cats also showed firing rate of CbN cells co-modulating with locomotion cycle (Armstrong and Edgley, 1984a). Similarly, recording from awake normal and dystonic rats also showed discrepancy in firing pattern of CbN cells, irregular firing is more evident in dystonic rats, suggesting well controlled of CbN cells activity is necessary for normal motor behavior (LeDoux et al., 1998). In addition to coordinating ongoing motor behavior, indirect excitation of CbN cells via suppression of inhibition on CbN cells with optical stimulation in mice could also initiate movement such as eye-lid closure or limb movement (Heiney et al., 2014a; Lee et al., 2015). Moreover, the cerebellar nuclei is also necessary for motor learning; for example, small GABAergic nucleo-olivary cells are suggested to be crucial for extinction of cerebellum dependent eye-lid closure conditioning (Medina et al., 2002) while CbN cells are suggested to be crucial for expression of conditioned responses (Heiney et al., 2014b).

1.1.1 Purkinje cells projection

CbN cells receive their major synaptic inhibition from intra-cerebellar cortical Purkinje cells and excitation from extra-cerebellar mossy fibers (see **Figure 1.1** for diagram of the simplified

cerebellar circuit). Synaptic inhibition comes from Purkinje cells. The cell bodies of Purkinje cells are located in the Purkinje cell layer of the cerebellar cortex, extend their dendrites to the molecular layer of the cerebellar cortex, and send their inhibitory axons to the cerebellar nuclei. In the circuit, like CbN cells, Purkinje cells cell also indirectly receive excitation from mossy fibers via granule cells, which are located in the granule cell layer and send ascending axons that bifurcate into parallel fibers and synapse onto Purkinje cells. In addition, Purkinje cells directly receive excitation from climbing fibers from inferior olivary neurons in the brainstem, which are suggested to encode error messages and which are involved in cerebellar motor control. All three layers: the granule cell layer, the Purkinje cell layer, and the molecular layer compose the cerebellar cortex, which integrates information from extra-cerebellar mossy fibers and climbing fibers and sends inhibitory inputs via Purkinje cells.

1.1.2 Mossy fibers projection

Unlike synaptic inhibition of CbN cells, synaptic excitation from mossy fibers comes from diverse brain regions; they project to different cerebellar nuclei and are suggested to encode different types of sensorimotor information. The cerebellar nuclei are composed of three pairs of nuclei from the lateral to the medial: the dentate nucleus, the interpositus nucleus, and the fastigial nucleus. The interpositus and fastigial nucleus, along with their related cerebellar

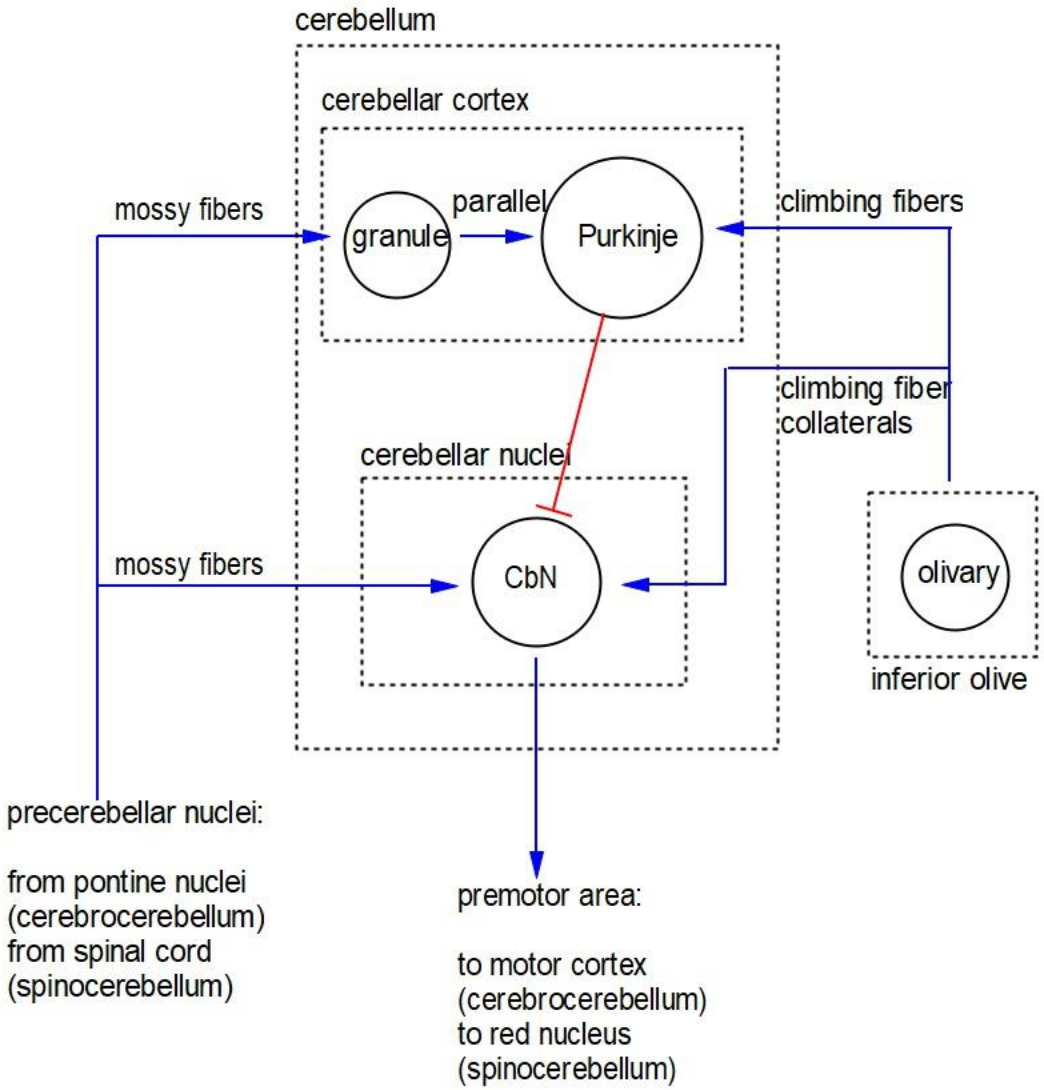

Figure 1.1. Diagram of the simplified cerebellar circuit diagram.

Diagram of the simplified cerebellar circuit. *Blue* line, synaptic excitation. *Red* line, synaptic inhibition.

cortical structures, the medial part of the hemisphere and vermis, are called spinocerebellum because they receive many mossy fiber inputs from the spinal cord and are mostly involved in regulating eye, body, and limb movements (Robinson and Fuchs, 2001; Miller et al., 2002; Raghavan and Lisberger, 2017). Somatosensory information such as touch, pressure, and limb position is transmitted to the interpositus and fastigial nucleus from spinal neurons through the spinocerebellar tracts either directly or indirectly through precerebellar nuclei; this information contains not only sensory feedback but also motor efference copy (Oscarsson, 1965; Bosco and Poppele, 2001; Azim et al., 2014). Sensorimotor information that is integrated in interpositus and fastigial nucleus is further sent to downstream nuclei such as the red nucleus for controlling body and limb movement.

The dentate nucleus and the related lateral cerebellar hemisphere are called the cerebrocerebellum; it receives mossy fiber inputs from the cerebral cortex, which is suggested to be involved in motor planning and cognition (Schmahmann, 1991). Cerebral cortical information is relayed by the pontine nuclei and transmitted to the cerebellum via the pontocerebellar tract (Brodal, 1978); this information is integrated in the dentate nucleus and is transmitted out of the cerebellum to the motor cortex and inferior olive, and is proposed to be involved in mental rehearsal and motor learning (Onodera, 1984; De Zeeuw et al., 1998).

However, not all information projected out of the cerebellum is through the cerebellar nuclei. The vestibulocerebellum, which is composed of the flocculonodular lobe, processes

proprioceptive information such as head's position in the cerebellar cortex from mossy fibers of different relay precerebellar nuclei such as vestibular nuclei (Gacek, 1968; Carpenter et al., 1972; Wilson et al., 1972; Kawato and Gomi, 1992) and directly projects out of the cerebellum through Purkinje cells to the vestibular nuclei in the brainstem; it is suggested to be involved in regulation of balance, vestibular reflexes, and eye movement. (Gacek, 1968; Robinson and Fuchs, 2001; Angelaki and Yakusheva, 2009; Schniepp et al., 2014; Kodama and du Lac, 2016).

1.2 Modulation of cerebellar nuclear cell output

Since CbN cells are the final output of the cerebellum, regulation of CbN cell spiking is important for shaping cerebellar output. At the cellular level, activity of CbN cell could be affected by three major factors: the intrinsic excitability of the CbN cells, the mossy fibers excitation, and the Purkinje cells inhibition. For excitatory and inhibitory synaptic inputs, there are many variables that may regulate CbN cell activity: the rate or temporal structure of the inputs, the number or the convergence of the inputs, and properties such as the synaptic strength and kinetics. The rate and temporal structure may change the regularity of CbN cells spontaneous firing, if it occurs, while the convergence ratio and synaptic strength may decide how much excitation or inhibition is required for regulating the activity of CbN cells; all these different variables may shape CbN cells activity to different degrees.

1.2.1 Firing properties of CbN cells, mossy fibers, and Purkinje cells

CbN cells are constantly active; they fire action potentials spontaneously and rapidly without synaptic transmission (Jahnsen, 1986; Mercer et al., 2016). The property of spontaneous firing may be due to the combination of low density of leak potassium channels, which leads to a relatively depolarized resting membrane potential at near -40 mV, the sodium channels with resurgent kinetics that permit rapid recovery of a subset of sodium channels, and the rapidly deactivating potassium currents that limit the AHP (Raman et al., 2000; Afshari et al., 2004).

Mossy fibers originate from several precerebellar nuclei such as pontine nuclei or vestibular nuclei in the brain stem (Kolkman et al., 2011). Possibly because of the heterogeneity of mossy fiber composition, reports of the characteristics of mossy fibers such as firing rate or firing pattern are highly variable; this variation may reflect encoding of different types of sensorimotor information from either the periphery or the cerebral cortex. For example, mossy fibers that convey sensory information of whisker were reported as showing burst firing, while mossy fibers that transmit sensorimotor information during locomotion were reported as showing stationary firing (Rancz et al., 2007; Powell et al., 2015). In addition to having different temporal structures, a large range of rates of mossy fiber firing is also reported, from tens to hundreds of spikes/sec (van Kan et al., 1993a; Arenz et al., 2008). Although mossy fibers encode different sensorimotor information, which is reflected by their heterogeneity of firing rate and firing pattern, their intrinsic properties might not be very different from each other. *In vitro* whole cell recording from different precerebellar neurons in mice showed that several intrinsic properties such as resting membrane potential, input-output firing curve, or action potential width are not

significant different from each other, suggesting some degree of similarity of their intrinsic excitability between different mossy fibers (Kolkman et al., 2011). In addition, different mossy fibers showed a similar capability of firing at high rates up to hundreds of spikes/sec; this could come from the combination of K_{v1} and K_{v3} potassium channels which allow fast repolarization, along with rapidly inactivating sodium channels for metabolic efficiency (Kolkman et al., 2011; Ritzau-Jost et al., 2014).

Purkinje cells, like CbN cells, also fire their action potentials spontaneously at high rates, which depends on the interaction of specialized sodium and potassium channels (Raman and Bean, 1997, 1999; Khaliq et al., 2003); this type of action potential is called a simple spike. The rate of simple spikes can be further modulated by activation of parallel fibers; activation of parallel fibers showed direct excitation and feedforward inhibition of Purkinje cells, which could occur through interneurons in the molecular layer, on the Purkinje cells (Mittmann et al., 2005; Mittmann and Häusser, 2007; Dizon and Khodakhah, 2011). In addition to simple spikes, Purkinje cells can also fire another type of action potential, the complex spike, which is from strong synaptic excitation from inferior olivary climbing fiber (Eccles et al., 1964; Schmolesky et al., 2002); complex spikes are composed of a burst of sodium spikes and spikelets that originate from the soma or initial segment of the axon along with the subsequent plateau potential, which is suggested to be from climbing fibers EPSC and depolarization in the dendrites (Khaliq and Raman, 2005; Monsivais et al., 2005; Davie et al., 2008).

1.2.2 Synaptic properties of mossy fibers excitation of CbN cells

Mossy fibers to CbN cell synapses have been proposed to be modulated during cerebellar learning (Medina and Mauk, 1999). Therefore many studies have been focused on *in vitro* synaptic plasticity (Pugh and Raman, 2006; Zhang and Linden, 2006; Person and Raman, 2010); these studies suggest that plasticity could be induced at these synapses with Purkinje cells as the modulators. In contrast, systematic examination of unitary synaptic properties and the convergence ratio has been less studied. One of the first studies done in younger mice (P4-11) at room temperature showed that mossy fiber EPSCs were largely composed of an NMDA receptor component (80%) along with a small AMPA receptor component (20%); the kinetics of AMPA and NMDA receptors also showed relatively slow kinetics of 7 ms and 20/136 ms (fast/slow component) respectively (Anchisi et al., 2001). However, one study using *in vitro* whole cell recording from Purkinje cell to CbN cells synapses at different temperature in mice showed that IPSCs have faster kinetics at higher temperature suggesting temperature could affect the kinetics of the synaptic response (Person and Raman, 2012b). Alternatively, synaptic structure and physiology might also change during development. Therefore, in order to study synaptic integration on CbN cells, it is necessary to measure the synaptic properties of mossy fiber to CbN cell synapses in older animals at near physiological temperature as well as to estimate of the convergence ratio that is also lacking in the literature.

Although there are only few studies looking at mossy fiber properties at synapses onto CbN cells synapses, many studies of mossy fibers have been done on mossy fiber synapses onto granule cells. These probably are not exactly the same as synapses onto CbN cells, but might still give

some hints to the mechanisms of information encoding, since CbN cells and granule cells may share the same mossy fibers inputs. Structurally, myelinated mossy fibers enter the granule cell layer and synapse onto granule cells as well as interneurons such as Golgi cells and unipolar brush cells (Chan-Palay, 1977); Golgi cells and unipolar brush cells further synapse onto granule cells and may be involved in feedforward inhibition and excitation (Dino et al., 2000; Nunzi et al., 2001; Mugnaini et al., 2011). Each mossy fiber forms several branches and features many boutons along its axon; on average, each mossy fiber makes synaptic contacts to ~50 granule cell dendrites (Jakab and Hamori, 1988). The mossy fiber bouton is large and makes a rosette like glomerulus around a dendrite of a granule cell. This structure is not found at CbN cell synapses (Chan-Palay, 1977). Electron microscopy studies also suggested that mossy fiber boutons have many release sites (Xu-Friedman and Regehr, 2003), which may support the capability of transmission during high frequency firing as previous described. While each mossy fiber makes synaptic contacts onto many granule cells, each granule cell has ~4 short dendrites and each dendrite is contacted by only one mossy fiber bouton. The EPSC from stimulating a single mossy fiber is ~50 pA, which is composed of both AMPA receptors and NMDA receptors (Silver et al., 1992; Rancz et al., 2007; Ritzau-Jost et al., 2014). Pharmacological studies from P11-17 rats at room temperature separating the AMPA receptor and NMDA receptor component showed a fast AMPA receptor EPSC with a decay time constant around 1 ms and a slower NMDA receptor EPSC with a decay time constant around 50 ms (Silver et al., 1992). Although the mossy fiber EPSC is relatively small, the activation of a single mossy fiber often stimulates the granule cell to fire (Rancz et al., 2007). This large response may come from the high membrane resistance of granule cells; one study also showed that short dendrites of granule cells share a high membrane resistance, which makes granule cells electrotonically compact and very responsive to mossy

fiber inputs (Delvendahl et al., 2015). Overall, these studies suggest that granule cells only receive ~4 mossy fibers but are responsive to mossy fiber excitation.

1.2.3 Synaptic properties of Purkinje cells inhibition of CbN cells

The synaptic properties of Purkinje cells have been well studied from different ages of mice at different recording temperatures (Anchisi et al., 2001; Person and Raman, 2012b); one study from our lab using *in vitro* recording from P17-26 mice at physiological temperature showed that the IPSC has a unitary conductance near 10 nS with a very fast decay time constant of 2.5 ms (Person and Raman, 2012b). In addition, the convergence ratio of Purkinje cells to CbN cells has also been carefully estimated from both morphological and physiological data showed an average of ~40 Purkinje cells converging onto CbN cells (Person and Raman, 2012b). The fast kinetics of IPSC and the high convergence ratio raise the possibility that regulation of CbN cells activity may be sensitive to the relative temporal structure and number/population of ongoing Purkinje cells activity. In fact, direct extracellular recording of the activity of Purkinje cells and their target CbN cells from decerebrate unanesthetized cats showed no consistent relationship in their firing rates (McDevitt et al., 1987), suggesting that the firing rates of single Purkinje cell afferent may not predict the firing of CbN cells. Moreover, population recordings from Purkinje cells and CbN cells from monkeys and cats showed both cells could co-modulate their firing activities during movement (Thach, 1970a, b; Armstrong and Edgley, 1984b, a). These observations lead to the idea that, even though inhibition by Purkinje cells is powerful, factors other than the firing rate of a single afferent Purkinje cell regulate the activity of CbN cells.

1.3 Purkinje cell synchrony

One of the possible attributes of population activity that may regulate CbN cells firing is the synchrony; in fact, Purkinje cells synchrony, for both simple spikes and complex spikes, has been recognized for a long time (Bell and Grimm, 1969; Bell and Kawasaki, 1972; Sasaki et al., 1989). A previous *in vitro* study from our lab also showed that by regulating the temporal structure of the Purkinje cells IPSPs, the spontaneous CbN cells activity could be suppressed by desynchronized IPSPs or recovered after relief of synchronized IPSPs, suggesting that synchrony might be one of the variables that regulates CbN cells activity (Person and Raman, 2012b).

1.3.1 Complex spike synchrony

Purkinje cell synchrony can be further divided into the complex spike synchrony and simple spike synchrony; these two forms of synchrony may be different in their temporal pattern and their modulation of CbN cell firing. Complex spike synchrony has long been recognized *in vivo* during different behaviors (Van Der Giessen et al., 2008; Mukamel et al., 2009; De Gruijl et al., 2014; Hoogland et al., 2015); for example, multi-electrode recordings from rats showed correlation of complex spikes synchrony to licking behavior (Welsh et al., 1995). The synchrony is often described physically as occurring in the area of 500 μm in the parasagittal direction. Temporally, the cross-correlations show peaks from 2 ms to tens of ms (Bell and Kawasaki, 1972; Sasaki et al., 1989; Wylie et al., 1995; De Zeeuw et al., 1997; Ozden et al., 2009). This complex spike synchrony may result in part from innervation of multiple Purkinje cells by a

common climbing fiber. Each climbing fiber can ramify its axon and make synaptic contacts to several Purkinje cells in the parasagittal plane. In addition, neighboring inferior olivary cells are electrically coupled at their dendritic spines by gap junctions composed of connexin 36, which further extends the range of the synchrony (Llinas et al., 1974; Sotelo et al., 1974; Llinas and Yarom, 1981; Bal and McCormick, 1997; Long et al., 2002; De Zeeuw et al., 2003). Olivary neurons often show synchronized subthreshold oscillation during rest, which is probably due to differential distribution of membrane conductances across their soma and dendrites, and can be regulated by excitatory and inhibitory synaptic drive (Llinas and Yarom, 1981; Khosrovani et al., 2007; Choi et al., 2010). The excitatory inputs from the midbrain and inhibitory inputs from GABAergic nucleo-olivary neurons increase or decrease the electrical coupling between olivary neurons respectively and further control the synchrony (de Zeeuw et al., 1990; Lefler et al., 2014; Turecek et al., 2014).

The effect of complex spike synchrony on CbN cells from *in vivo* recording from anesthetized rats showed prolonged inhibition ~100 ms of CbN cell activity (Blenkinsop and Lang, 2011). In addition, sometimes CbN cells could increase their firing shortly right before the strong silencing, which presumably could be from direct excitation from climbing fiber collateral (Blenkinsop and Lang, 2011; Tang et al., 2016).

1.3.2 Simple spike synchrony

In addition to complex spike synchrony, the literature also shows that Purkinje cells can independently fire their simple spikes in synchrony; this simple spike synchrony is also

correlated with different motor behaviors or associated with different kinds of sensory stimulation (Bell and Grimm, 1969; MacKay and Murphy, 1976; Ebner and Bloedel, 1981; De Zeeuw et al., 1997; Shin and De Schutter, 2006; Heck et al., 2007; de Solages et al., 2008; Bosman et al., 2010; Wise et al., 2010). However, simple spike synchrony shows many properties that are different from complex spike synchrony in terms of temporal structure and physical area, which implies different mechanisms underlying these two forms of synchrony. First, the most profound characteristic of simple spike synchrony is its highly precise temporal relationship; calculation of cross-correlation of synchronized Purkinje cells usually showed maximal correlation at less than 4 ms, which is more synchronized than complex spikes (Ebner and Bloedel, 1981). Second, the physical region in which simple spike synchrony occurs seems narrower than in complex spike synchrony; simple spike synchrony is usually reported when Purkinje cells are within 100 um (Bell and Grimm, 1969). The spatial pattern of synchronized Purkinje cells is also different from the one in complex spike synchrony. Whereas complex spike synchrony is often reported in the parasagittal plane, simple spike synchrony is reported in a mediolateral (coronal) pattern (MacKay and Murphy, 1976; Heck et al., 2007).

All these differences suggest a fundamental difference in mechanism between simple spike synchrony and complex spike synchrony. Unlike the relatively clear mechanism for complex spike synchrony, the mechanism for simple spike synchrony is still under debate; there are at least four hypotheses for generation of simple spike synchrony. The first hypothesis is relatively stronger synaptic excitation from granule cell ascending axons, as compared to parallel fiber axons. Granule cells axons ascend into the molecular layer and bifurcate into parallel fibers

which run transversely in the mediolateral direction. Each parallel fiber contacts numerous Purkinje cells and is expected to principally activate these Purkinje cells consecutively by a spreading wave of excitation, in which the speed of wave is probably proportional to the conduction velocity of the parallel fiber (Braitenberg and Atwood, 1958). However, while the transverse excitatory wave can indeed be induced by direct electrical stimulation of a parallel fiber beam (Gao et al., 2003), it is relatively sparse and weak under physiological conditions; one study trying to find the on-beam traveling wave but found synchronized simple spikes instead (Heck et al., 2007). This synchrony could be from relative stronger synaptic excitation from ascending axons than parallel fibers; in fact, several studies showed a synaptic difference between ascending axons and parallel fibers with morphological and physiological approaches. Electron microscopy studies showed a larger synaptic volume and more vesicles in ascending axons than in parallel fibers (Gundappa-Sulur et al., 1999); electrophysiological recordings in slices also reported that ascending axons have more functional synapses, higher release probability, and more resistance to long-term depression (Isope and Barbour, 2002; Sims and Hartell, 2005, 2006). Other studies, however, indicated that ascending axons are functionally equivalent to parallel fibers and showed no difference in unitary responses in Purkinje cells (Walter et al., 2009; Zhang and Linden, 2012).

Regardless of the relative synaptic strength between ascending axons and parallel fibers, Purkinje cells may still be preferably excited by the granule cells right beneath them by other mechanisms. The second mechanism comes from lateral inhibition by molecular layer inhibitory interneurons; these interneurons, such as stellate cells and basket cells, receive excitatory inputs

from parallel fibers and send their inhibitory axons to local Purkinje cells in a parasagittal or coronal direction. One study of rat cerebellar slices showed that stimulating granule cells led to excitation in Purkinje cells located directly above them but generated inhibition in Purkinje cells that located laterally in parasagittal planes (Dizon and Khodakhah, 2011). Other studies also suggested that stimulating granule cells produces feedforward inhibition in coronal direction that can narrow the excitation window for Purkinje cells and may increase the precision (Brunel et al., 2004; Mittmann et al., 2005; Kanichay and Silver, 2008; D'Angelo and De Zeeuw, 2009; Dizon and Khodakhah, 2011). The third mechanism, which is not mutually exclusive, comes from the lateral inhibition from adjacent Purkinje cells. One study showed that blocking GABA transmission, which presumably blocks inhibition from both molecular layer interneuron and adjacent Purkinje cells, disrupted simple spike synchrony. However, suppressing interneurons with a cannabinoid receptor agonist, which leaves the GABA transmission between adjacent Purkinje cells intact, preserved the synchrony, leading to the idea that lateral inhibition from Purkinje cells axon collateral may be crucial for synchrony (de Solages et al., 2008).

The last mechanism for regulating simple spike synchrony in fact comes from complex spike synchrony. Complex spike synchrony leads to Purkinje cells not only firing complex spikes simultaneously but also pausing simultaneously after complex spikes; the restarting of simple spikes following the pause is called phase resetting, which could also occur among Purkinje cells after a pause of concerted complex spikes and theoretically generate subsequent simple spike synchrony. The direct evidence for complex spike synchrony facilitating simple spike synchrony is still lacking; however, the co-occurrence of complex spike synchrony and simple spike

synchrony in certain cerebellar areas suggests a possible causal relation. For example, in the vestibulocerebellum, simple spike synchrony correlated to the complex spike synchrony during optokinetic reflex; the occurrence of simple spike synchrony also showed in the parasagittal plane as complex spike synchrony (De Zeeuw et al., 1997). In other cerebellar regions, such as Crus 2 and the paramedian lobule, which control whisker movements and reaching movements respectively, simple spike synchrony is largely restricted to the coronal plane and may be independent of complex spike synchrony (Heck et al., 2007; Bosman et al., 2010). These studies imply that different mechanisms of simple spike synchrony may be performed in different cerebellar regions and are not necessarily mutually exclusive.

In addition to the mechanism of simple spike synchrony, the physiological regulation of the synchrony on the CbN cells is not totally clear yet. *In vitro* recordings from our lab showed that with perfect synchrony of Purkinje cells IPSPs that were applied with dynamic clamp, CbN cells could firing their action potential at the ends of the concerted IPSPs (Person and Raman, 2012b). This is due to the fast kinetics of Purkinje cell IPSCs and the propensity for CbN cells to fire action potential spontaneously. Fast concerted IPSPs produce a strong inhibition but also provide a temporal window at the end of concerted IPSPs, permitting CbN cells to spike in the window because of their spontaneous firing property. In contrast, desynchronization of IPSPs could remove the window and lead to prolonged inhibition of CbN cells. In this case, the degree of synchrony might be one variable that interacts with the spontaneous firing property of CbN cells and regulates CbN cells activity. This phenomenon could also be elicited *in vivo* with direct stimulation of the molecular layer in anesthetized mice (Person and Raman, 2012b).

1.4 The Goal and experimental approach in this study

The observations from *in vivo* studies that Purkinje cells synchronize their simple spikes and from the *in vitro* study from our lab that CbN cell activity can be regulated by the degree of synchrony raises the possibility that the inhibitory synchrony might be a variable that influences overall synaptic integration on CbN cells. In this idea, the effect on the CbN cells would heavily rely on the number of Purkinje cells, the relative temporal structure of concerted simple spikes, and the unitary properties such as synaptic strength and the kinetics of the IPSPs. However, many questions still need to be answered in relation to this idea. For example, in the previous study, the synchronized IPSPs were either applied by dynamic clamp or direct stimulation, which produces perfect synchrony and might not exist in physiological condition; with what degree of precision (jitter) would the synchrony still provide enough window for CbN cells firing action potential? Another question may come from the interaction between inhibitory synchrony and mossy fiber excitation on regulating CbN cell activity; since mossy fibers directly excite CbN cells and indirectly excite Purkinje cells via granule cells, it is possible that the inhibition may overlap with mossy fiber excitation and co-control the activity of CbN cells. How does mossy fiber excitation interact with synchrony? One possibility is that mossy fiber will intensify the effects seen in previous experiment. In fact, injecting DC current to CbN cells showed the increase of spike probability while still preserving the temporal structure of synchrony (Person and Raman, 2012b). Again, whether the same observation would be seen physiologically might also rely on the synaptic property of mossy fibers.

In order to answer these questions in present study, the basic properties of mossy excitation in CbN cells were measured and applied with dynamic clamp along with different degrees and jitter of synchrony to investigate the interaction of excitation and inhibition in CbN cells. The locations of Purkinje cell synapses are largely somatic (Chan-Palay, 1977), which is also ideal for dynamic clamp. Dynamic clamp, also known as conductance clamp, introduces artificial conductances into cells to mimic circuitry as real biological environment. This technique was first introduced in 1993 for studying the stomatogastric ganglion in crabs and hippocampal neurons in rats (Robinson and Kawai, 1993; Sharp et al., 1993). As an intermediate connection between the computer and the amplifier, the dynamic clamp is more like an interface to command the amplifier to inject current into cells; thus, the dynamic clamp is still using the conventional amplifier to inject Cl^- current. Similar to voltage clamp, the dynamic clamp computes the difference between the measured membrane potential and command potential, which in the dynamic clamp is set as the reversal potential for each particular conductance, multiplies the driving force by the desired amount of conductance, and injects the resulting current into recording cells. In contrast to the conventional voltage clamp, the desired conductance of the dynamic clamp can be changed effectively; all the kinetics and the amplitude can be described in mathematical equations and altered with time and voltage in order to design time and voltage dependent conductances (Prinz et al., 2004).

Theoretically, the update rate of the dynamic clamp is fully dependent on the speed of the digital signal processing (DSP) board; the conductance cannot be injected faster than the speed limit of the board. Based on the number of outputs of the DSP board, multiple conductances can be

applied; the properties of each conductance are described by its own equation and can be applied simultaneously. The dynamic clamp can also be used along with other forms of external stimulation such as using the dynamic clamp to simulate synaptic inhibition while electrically stimulating synaptic excitation. In this study, we used SM-2 digital conductance injection software running on a high speed P25M DSP board to simulate mossy fiber EPSPs and Purkinje cell IPSPs on CbN cells (Robinson, 2008).

Despite the convenience of injecting artificial conductances, the dynamic clamp also has its own limits; generally, there are three major limitations that the dynamic clamp has. The first limitation is although the conductance can be described to simulate different channels, the ion that actually injected into cells is still Cl^-; because of this, the dynamic clamp can only to be used to mimic the fluctuation of the membrane potential. For example, using the dynamic clamp to apply NMDA receptor can only generate the depolarization of the membrane potential but loses the potential Ca^{2+} dependent biochemical pathway. The second limitation is the restricted injection site. Since the dynamic clamp uses the recording pipette to inject current, the injection site is restricted primarily to the soma. As a result, synaptic potentials from the distal dendrite cannot be mimicked by the dynamic clamp because the injection from the soma would inevitably produce shunting of the cells. This limitation can, however, be reduced by either dendritically recording or applying conductances with a high reversal potential along with conductance to maintain the driving force and reduce the shunting effect. The final limitation comes from the essential point that the dynamic clamp is still using the conventional amplifier to apply conductances. Every artifact that could affect clamp quality such as series resistance error would

also affect the accuracy of the conductance; this limitation can be reduced by using low resistance pipettes to decrease the artifact.

Nevertheless, with dynamic clamp, the interaction of mossy fiber excitation and Purkinje cells synchrony on CbN cells can be measured systematically in a controlled *in vitro* experimental environment. Finally, the mossy fiber properties measured in this study can serve as the parameter for future modeling studies and the integration of mossy fibers excitation and Purkinje cells synchrony may hopefully provide the possible cellular mechanism for ongoing *in vivo* synchrony studies.

The following chapter has been published as:

Wu, Y., Raman, I.M. (2017). Facilitation of mossy fibre-driven spiking in the cerebellar nuclei by the synchrony of inhibition. *Journal of Physiology* May 17. doi: 10.1113/JP274321.

Chapter 2: Facilitation of mossy fiber-driven spiking in the cerebellar nuclei by the synchrony of inhibition

2.1 Introduction

The action potential firing patterns of large neurons of the cerebellar nuclei (CbN cells), which form the primary cerebellar projections to premotor areas, help coordinate and correct movements. CbN cells fire spontaneously at high rates (Jahnsen, 1986; Raman et al., 2000), and their activity is regulated by strong inhibition from rapidly firing, convergent cerebellar Purkinje neurons. The activity of CbN cells is additionally controlled by synaptic excitation from cerebellar mossy fibers, which send sensorimotor signals to the cerebellum (Eccles et al., 1974; McCrea et al., 1977; Wu et al., 1999). Mossy fibers also indirectly control Purkinje cell activity via granule cells. Thus, Purkinje and mossy fiber inputs to CbN cells are both likely to be modulated during cerebellar behaviors (Armstrong and Edgley, 1984b, a; Powell et al., 2015). The overlapping input from both sources raises the question of how inhibitory and excitatory synaptic potentials interact to modulate CbN cell firing, thereby generating the signals necessary for precise motor control.

One possibility is that inhibition and excitation simply oppose one another, so that the dominant variable controlling CbN cell output is the relative firing rate of convergent Purkinje cells and mossy fibers. Another possibility, which is not mutually exclusive, is that temporal aspects of synaptic signals are also relevant (Gauck and Jaeger, 2000). Effects of synaptic timing seem worth investigating because *in vivo* studies of cats and rodents report that Purkinje cells can fire

simple spikes nearly simultaneously (Bell and Grimm, 1969; MacKay and Murphy, 1976; Ebner and Bloedel, 1981; Heck et al., 2007; de Solages et al., 2008; Wise et al., 2010; De Zeeuw et al., 2011), which may synchronize subsets of IPSPs in CbN cells. In recordings from cerebellar slices with excitation blocked, we previously found that CbN cells can indeed respond to inhibitory synchrony. IPSPs effectively suppress CbN spikes, but because the intrinsic excitability of CbN cells is so strong, the offset of coincident IPSPs provides a gap in which firing probability is elevated. Consequently, CbN cells phase-lock to the subpopulation of synchronized IPSPs, and firing rates depend not only on the rate but the synchrony of inhibition (Person and Raman, 2012b).

Synaptic excitation, however, likely alters the responses of CbN cells to either synchronous or asynchronous inhibition. How it does so will depend on the properties of excitatory synapses, including the amplitude and kinetics of AMPAR and NMDAR EPSCs activated by mossy fiber inputs, as well as the convergence of mossy fibers onto CbN cells. We therefore measured basic properties of excitatory inputs to CbN neurons in cerebellar slices from weanling mice and then used dynamic clamp (Robinson, 2008) to explore the interaction of physiologically plausible rates and patterns of excitation and inhibition. The results demonstrate that increasing inhibitory synchrony permits a fixed amount of excitation to drive higher rates of more precisely timed action potentials. Conversely, increasing inhibitory asynchrony more effectively overrides excitation. Thus, the degree of Purkinje synchrony regulates the efficacy of mossy fiber excitation of CbN cells, influencing both the rate and timing of cerebellar output.

2.2 Materials and Methods

Ethical Approval. All procedures conformed to NIH and institutional guidelines and were approved by the Northwestern University IACUC. Methods of euthanasia were consistent with the recommendations of the Panel on Euthanasia of the American Veterinary Medical Association. The research complies with the policies of *The Journal of Physiology* as detailed in (Grundy, 2015).

Preparation of cerebellar slices. Experiments were done on cerebellar slices from C57BL/6 male and female P17-23 mice (Charles River; Telgkamp & Raman, 2002; Person & Raman, 2012a). Mice were housed in Northwestern's accredited animal care facility with *ad lib* access to food and water. For experimentation, animals were selected randomly without regard to sex, but sexes are reported with N-values, and sex differences were considered as described below. Mice were anesthetized by isoflurane inhalation until unresponsive to toe pinch and transcardially perfused with warmed (35°C) artificial cerebral spinal fluid (ACSF) containing (in mM): 123 NaCl, 3.5 KCl, 26 NaH_2CO_3, 1.25 NaH_2PO_4, 10 glucose, 1.5 $CaCl_2$, 1 $MgCl_2$, oxygenated with 95/5% O_2/CO_2. Mice were decapitated, the cerebellum was removed, and parasagittal cerebellar slices (300 μm) were cut on a vibratome (Leica VT1200) in oxygenated ACSF at 35°C (Person and Raman, 2012b). Cutting slices at warm temperatures (Oertel, 1983, 1985; Trussell et al., 1993; Zhang and Trussell, 1994a, b; Gardner et al., 1999) preserves slices with heavily myelinated fibers, presumably by preventing the myelin from hardening as it does at cold temperatures and shattering and/or stretching the tissue as the blade passes through it. Slices were incubated in oxygenated ACSF at 35°C for 30 to 45 min and then maintained at room temperature until use.

Electrophysiology. Slices were transferred to a chamber on an AXIO Examiner A1 microscope (Zeiss) and perfused with ACSF at 32-35°C (see details on temperature below) with a TC-324B automatic temperature controller (Warner Instrument Corporation). The CbN contain many kinds of neurons, which differ in their morphology, transmitter content, molecular makeup, physiological properties, and targets (Chan-Palay, 1977; Molineux et al., 2006; Uusisaari and Knopfel, 2012; Husson et al., 2014; Zhou et al., 2014; Najac and Raman, 2015; Canto et al., 2016). To reduce variance across recordings and to maximize the validity of comparisons with previous experiments (Person and Raman, 2012b; Mercer et al., 2016), large CbN cells were selected for recording based on visual identification by their size (20-25 μm somatic diameter) and location 1.3 mm to 1.9 mm from the cerebellar midline. Most of these neurons were in the anterior interpositus nucleus, with some cells in the posterior interpositus or medial portion of the lateral nucleus. Whole-cell recordings were made with glass pipettes (3-6 MΩ, pulled on a Sutter Instruments P97 puller PMC and positioned with an SD Instruments 1000e micromanipulator) with a Multiclamp 700B amplifier (Molecular Devices). Series resistances were 11.0 ± 0.4 MΩ (N=109) and were monitored for stability throughout the experiment. No compensation was applied in voltage-clamp experiments; the bridge was balanced in current-clamp experiments. Cells with series resistance changes >20% were discarded. Data were digitized at either 10 KHz (Figures 1-4, and Figure 5 for conditions with >100 mossy fibers) or 20 KHz (all other experiments) with a Digidata 1440A and recorded with pClamp software (Molecular Devices).

For current-clamp recordings, the intracellular solution contained (in mM): 120 K-gluconate, 2 Na-gluconate, 6 NaCl, 2 $MgCl_2$, 0.1 $CaCl_2$, 1 EGTA, 4 MgATP, 0.3 Tris-GTP, 14 Tris-creatine phosphate, 10 HEPES, adjusted to 293 mOsm with sucrose and pH 7.35 with KOH. For voltage-clamp recordings, the intracellular solution contained (in mM): 120 $CsMeSO_3$, 3 NaCl, 2 $MgCl_2$, 1 EGTA, 4 MgATP, 0.3 Tris-GTP, 14 Tris-creatine phosphate, 10 HEPES, 1.2 QX-314 (N-(2,6-dimethylphenylcarbamoylmethyl)-triethylammonium bromide), 4 TEA-Cl, 12 sucrose, adjusted to 288 mOsm with sucrose and pH 7.32 with CsOH. In all experiments, SR95531 (10 μM) was added to the ACSF to block $GABA_A$ receptors. In the current-clamp experiments of Figures 4-7, strychnine (2 μM) was included along with SR95531 to block glycine receptors in addition to $GABA_A$ receptors, although no evidence of glycinergic transmission was evident in any experiments. As noted, the extracellular ACSF was further supplemented with 10 μM DNQX (dinitrofiquinoxaline-2,3-dione) to block AMPA receptors or 10 μM CPP ((RS)-3-(2-carboxy-piperazin-4-yl)-propyl-1-phosphonic acid) to block NMDA receptors. Chemicals were from Sigma-Aldrich (St. Louis, MO) except DNQX, CPP, and SR95531 were from Tocris Cookson. A liquid junction potential of 4 mV was measured and is corrected for in all reported voltages.

For experiments involving electrically evoked synaptic responses, mossy fibers were stimulated with 100 μs current pulses of 10 μA - 10 mA applied with a concentric bipolar electrode (FHC) positioned in the inferior cerebellar peduncle near the CbN, controlled by an ISO-flex stimulus isolation unit (A.M.P.I) and a Master-8 controller (A.M.P.I). Since mossy fibers are heterogeneous and may differ physiologically (Kolkman *et al.*, 2011; (Chabrol et al., 2015), the stimulation electrode was positioned as consistently as possible to maximize replicability and

reliability. The stimulation electrode may activate climbing fiber collaterals as well as mossy fibers; however, the extent of depression was not consistent with activation of a preponderance of climbing fiber collateral inputs (see *Results*). For measures of depression, the start-to-start interval was 5 sec. At each of 6 frequencies, 5 sweeps were averaged and normalized to the peak of the first EPSC. For current-clamp experiments with evoked EPSPs and dynamically clamped inhibition, single sweeps included 3 test periods of 200 ms, each separated by 700 ms. During the interval preceding each test period, firing was suppressed by dynamically clamped inhibition from 40 asynchronous inputs, each at 50/sec. On successive sweeps, EPSPs were alternately evoked or not evoked during the test periods, with 90 Hz EPSPs in the first, 133 Hz in the second, and 160 Hz in the third period. Over the series of experiments we realized that the prolonged periods of low firing during asynchronous inhibition led to a slow activation of I_h, which slightly depolarized the cell over subsequent test periods. This onset of I_h accounts for the slightly higher frequency of mean basal firing for higher stimulation rates even in the "no EPSP" controls. Because comparisons were made for interleaved trials in a fixed stimulation period, each stimulation rate had its own control and no correction was necessary.

Unitary conductances were calculated by dividing unitary EPSC amplitudes by driving force estimated from the holding voltage and the measured reversal potential. Reversal was +15 mV for AMPARs and +30 mV for NMDARs. These positive values might result in part from factors such as the higher extracellular concentration of permeant ions and their relative permeability, but imperfect space clamp may also have contributed. If the true reversals were closer to zero and clamp error was greater at more positive voltages, the unitary conductances would have been

underestimated for AMPAR EPSCs (recorded at -74 mV) and overestimated for NMDAR EPSCs (recorded at +86 mV). The different polarities might have approximately canceled these errors in the physiological estimate of convergence and in measurements of the effect of excitation in the face of inhibition.

All experiments that involved electrical activation of mossy fibers, measurement of synaptic properties, and initial dynamic clamp experiments (Figures 2.1-2.4) were done close to 35°C, to facilitate comparison with previous work (Person and Raman, 2012b). The temperature of each recording was measured with a thermistor and was 34.7° ± 0.1°C (N=74) in these experiments. The kinetics of the injected synaptic conductances in dynamic clamp therefore all represented measurements made near 35°C. For the dynamic clamp experiments of Figures 2.5-2.7, longer recordings with multiple replicates on a single cell were required. Because recording durations could be prolonged by slightly lowering the temperature, these recordings were made at a mean recording temperature of 33.3° ± 0.3°C (N=35). This difference may have slowed the kinetics of intrinsic channels by ~60% (assuming a Q10 of 3) but had no substantial difference on spontaneous firing rates, which were 116 ± 5 Hz at 33.9° ± 0.2°C (N=25) and 117 ± 18 Hz at 32.0° ± 0.1°C (N=9, $p=0.95$). This lack of a strong temperature dependence of firing rate is consistent with previous measurements in Purkinje cells (Khaliq et al., 2003).

Estimation of convergence for dynamic clamp studies. To estimate an anatomically plausible degree of convergence to test in dynamic clamp studies, calculations were made from anatomical

measurements as in (Person and Raman, 2012b). The surface area of GAD-negative large CbN cells in mice was estimated from data from Uusisaari et al. (2007). Choosing values from the high end of the distribution, we calculated the surface area for 4 dendrites of 190 µm length and 2 µm diameter (ignoring 10 µm of thicker proximal dendrite innervated almost exclusively by Purkinje cells) to be ~4775 μm^2. Most excitatory synapses are made on this region of the dendrites, but the extent of innervation can vary greatly; in the rhesus monkey, 20-95% of the dendrites can be covered with synapses giving ~1000-4500 μm^2 of innervated membrane (Chan-Palay, 1977). About 20% of the input comes from mossy fibers (Chan-Palay, 1977, Fig. 4-27), which gives 200-900 μm^2 of CbN dendritic membrane with mossy fiber synapses. The diameter of mossy fiber swellings in the rat is 1-1.7 µm (Wu et al., 1999); assuming a circular contact, these diameters give 0.7-2.26 μm^2 for a boutonal cross-sectional area, which we round down to 0.5-2 μm^2 for the synaptic contact area. At the low end, 200 μm^2 innervated membrane ÷ 2 μm^2 boutons = 100 mossy fiber boutons; at the high end, 900 μm^2 innervated membrane ÷ 0.5 μm^2 boutons = 1800 mossy fiber boutons per CbN cell. The number of boutons per cell can be estimated from the quantal content and release probability. The rare spontaneous EPSCs observed were about half the amplitude of the unitary responses (0.53 ± 0.05 nS, ratio to unitary conductance in each cell, 0.49 ± 0.08, N=6); if these were mEPSCs, the quantal content could be near 2. If the release probability were 0.4-0.66, each mossy fiber might have 3-5 boutons contacting each CbN cell. Dividing the number of mossy fiber boutons per CbN cell by the number of boutons per mossy fiber to get 100/5 at the low end and 1800/3 at the high end to get a rough estimate of 20-600 mossy fibers per CbN cell. It is necessary to note that several of these parameters are only weakly constrained or highly variable, such as the number of dendrites, the extent of innervated membrane, the release probability, and the number of boutons per mossy

fiber per CbN cell. Nevertheless, they at least suggest that reasonable degrees of convergence to test would range from several tens to a few hundred mossy fiber afferents per CbN cell.

Dynamic clamp. Conductance or "dynamic" clamp (Robinson and Kawai, 1993; Sharp et al., 1993; Robinson, 2008) was used to inject conductances to generate synaptic potentials (dIPSPs and dEPSPs). Conductances were applied with SM-2 digital conductance injection software (Cambridge Conductance) running on a P25M digital signal processor board (Innovative Integration). All parameters for excitatory and inhibitory conductances were taken from experimental measurements of unitary amplitudes and kinetics made either in the present experiments for excitation, or in the same preparation as used here for inhibition (Person and Raman, 2012b). For dIPSPs that mimicked Purkinje cell inputs, the unitary conductance was set at 5 nS (accounting for 50% depression from the peak unitary amplitude) with a rise time of 0.1 ms, decay time constant of 2.5 ms, and reversal potential of -68 mV. Because 30-50 Purkinje cells converge onto each CbN cell (Person and Raman, 2012b), the number of inhibitory inputs was held constant at 40 in all experiments. For dEPSPs, both AMPAR and NMDAR conductances were applied concurrently through the dynamic clamp with parameters measured in the present experiments. Because the dynamic clamp software defined the rise time with an exponential time constant, the data were fit to obtain this parameter, the value of which is briefer than the 10-90% rise times reported in the text. The conductances underlying AMPAR dEPSPs were set to have a rise time constant of 0.28 ms and decay time constant of 1.06 ms, with a reversal potential of 11.5 mV. As indicated, synaptic depression was accounted for by scaling the unitary amplitude by 0.45 (for 20-Hz trains), or 0.396 nS (for >20-Hz trains). The conductances

underlying NMDAR dEPSPs were set to have a rise time constant of 1.9 ms and decay time constant as 7 ms, with the reversal potential of 32.4 mV; the unitary conductance was set at 0.57 (no depression), 0.285 (20-Hz trains), 0.228 nS (>20-Hz trains).

A complication of dynamic clamp is that excitatory and inhibitory synaptic conductances are injected into the soma, where they are shunted by each other and the somatic voltage-gated conductances. This situation is appropriate for the inhibitory conductance, since Purkinje synapses are largely somatic (Chan-Palay, 1977). Some excitatory synapses also overlap with inhibitory synapses, particularly on the more proximal dendrites, but some excitatory input is also further out on the dendrites, where it may not be subject to shunting. In the extreme case of no shunting, it would be best mimicked by direct current injection that is invariant with voltage, rather than dynamic clamp (e.g. Mittmann & Häusser, 2007). Therefore, where noted, shunting of dEPSPs by dIPSPs was reduced by increasing the driving force at -50 mV fivefold by positively shifting the reversal potentials (to +257.5 mV for AMPAR and +362 mV for NMDAR EPSCs) and decreasing the conductance fivefold to maintain the unitary current expected at the soma at -50 mV. These changes made the excitatory current fluctuate by <20% in the range of voltages traversed by action potentials (-70 to +10 mV), decreasing the shunt by >80%.

The event times of dIPSPs and dEPSPs were generated offline in Igor Pro (WaveMetrics). For synchronous inputs, the unitary conductance was scaled by the number of inputs that we wished to synchronize, and injected accordingly at the desired rate. For asynchronous inputs, event times

for individual inputs were generated from a Gaussian distribution with a mean of the desired interval and a CV of 1. Thus, for asynchronous inputs, although all inputs have the same mean firing rate, the firing patterns are irregular. Because a true Gaussian with a mean interval corresponding to the inverse rate (e.g., 20 ms for 50 events/sec) and a CV of 1 necessarily generates negative intervals, the negative event times were removed and the peak of the Gaussian was shifted accordingly to give the desired mean event rate. The trains for individual inputs were then merged to represent the population event times and used to trigger injection of asynchronous conductances.

Generating trains of high-frequency asynchronous spike times tended to produce a high probability of overlapping events. These did not sum in the dynamic clamp system, leading to an understimulation relative to the desired frequency. Therefore, in Figures 2.5-2.7, overlapping events were identified offline and separated by 100 μs to minimize understimulation, and, where the accumulation of 100 μs shifts made the time interval to accommodate all the stimuli deviate from the desired frequency, the plots were corrected to illustrate the actual rate of inputs applied. For experiments mimicking >100 mossy fibers, it was impossible to ensure that every input occurred at a distinct time. To ensure that the appropriate total excitatory conductance was injected, we scaled the unitary conductance by 10 and generated event times for one-tenth of the number of desired inputs. Thus, 200, 400, or 800 inputs were mimicked as 20, 40 or 80 independent clusters of 10 simultaneously occurring inputs.

Because the spontaneous firing rate of Purkinje cells is near 50 spikes/sec (e.g., Häusser & Clark, 1997), the basal rate for each of the 40 inhibitory inputs was set at 50 IPSPs per second. Rates of asynchronous inputs are reported with units "/s" and rates of synchronous inputs, which were always perfectly regular, are reported with units "Hz." The two parameters that were varied were the proportion of inputs that synchronized (0%, 5%, 10%, 25%, or 50%, corresponding to 0, 2, 4, 10, or 20 synchronized inputs) and the precision of synchrony or jitter. In experiments testing the effects of jitter, event times corresponding to near-synchronous IPSPs were drawn randomly from distributions with the desired standard deviations (0.5, 1, 2, 4 ms) about the mean desired event time; the jitter value is equal to the standard deviation. In the condition of 50% synchrony (20 inputs), the random generation of event times led to a high proportion of overlapping events, as described above. Because these events had to be separated by shifting each overlapping spike by 100 μs, a small but accumulating delay of the next stimulus in the train slightly prolonged the stimulus intervals beyond 10 ms. Therefore, in the analysis of the temporal patterns of CbN spikes with 50% inhibitory synchrony, we calculated the actual mean time of each synchronized event and corrected the interstimulus intervals accordingly. The corrected interstimulus intervals were also used for statistical analysis with the Rayleigh test.

Data analysis. The data were analyzed and plotted with Igor Pro software. Data are presented as mean ± SEM. Statistical significance was tested with repeated measures ANOVAs followed by paired or one-sample t-tests as indicated or Rayleigh's tests for non-uniformity, and *p*-values are reported. For Rayleigh's test, the unbinned spike times were first transformed into a polar graph by defining inter-stimulus interval as a circle and different spike times as different angles and

were tested with Rayleigh's test for non-uniformity. Because intrinsic and some synaptic properties of CbN cells are different in males and females (Mercer et al., 2016), all data was subjected to post-hoc examination for sex differences. For properties of excitatory inputs, no statistical differences were detected (conductance, time constant, rise time, or depression of EPSCs, $p>0.2$ all male-female comparisons). For firing rates with dynamically clamped inhibition, no statistical differences were found for asynchronous inhibition ($p=0.5$) or 50% synchrony ($p=0.14$). In the latter case, which had the lowest p-value of all male-female comparisons, firing rates were 5±3 Hz for males (N=12) and 13±4 Hz for females (N=10), consistent with a higher spontaneous rate in the absence of synaptic inhibition in females (Mercer et al., 2016). Since none of the differences were statistically significant, data were pooled between sexes, but numbers of cells from males (M) and females (F) are reported.

2.3 Results

Properties of mossy fiber-mediated EPSCs. With the goal of accurately mimicking mossy fiber-mediated EPSCs in dynamic clamp studies, we began by measuring the unitary amplitudes, kinetics, voltage dependence, and short-term plasticity of evoked AMPAR- and NMDAR-mediated synaptic currents in large CbN cells in cerebellar slices from weanling (P17-P23) mice. First, to investigate the properties of AMPAR unitary EPSCs (uEPSCs), large CbN cells were voltage-clamped at -74 mV in CPP and SR95531 (N=20; 11 M, 9 F; for 1 cell, strychnine was also present, with indistinguishable results). EPSCs were evoked electrically, and the stimulation strength was gradually decreased until a fixed intensity generated both successes and failures (**Figure 2.1A**, *top*), as predicted for a single afferent. Converting these uEPSC amplitudes to conductances gave a mean unitary conductance of 0.99 ± 0.13 nS. The kinetics were fast, with a 10%-90% rise time of 0.44 ± 0.07 ms and a decay phase that was well fit by a single exponential time constant (τ) of 1.06 ± 0.11 ms (**Figure 2.1A**, *bottom*).

For NMDAR responses, uEPSCs were recorded in DNQX and SR95531 at +86 mV (**Figure 2.1B**, *top*). The stimulus intensity was again decreased to a level that generated both successes and failures, and the unitary conductance, 10%-90% rise time, and decay time constant were measured (**Figure 2.1B**, *bottom, red symbols*, N=5). In 8 additional cells, minimal EPSCs could be measured, for which further reducing the stimulus intensity produced only failures, but no single level gave both successes and failures (**Figure 2.1B**, *bottom, black symbols*). For 6 of these cells, the minimal conductance was within 20% of the mean unitary conductance, helping

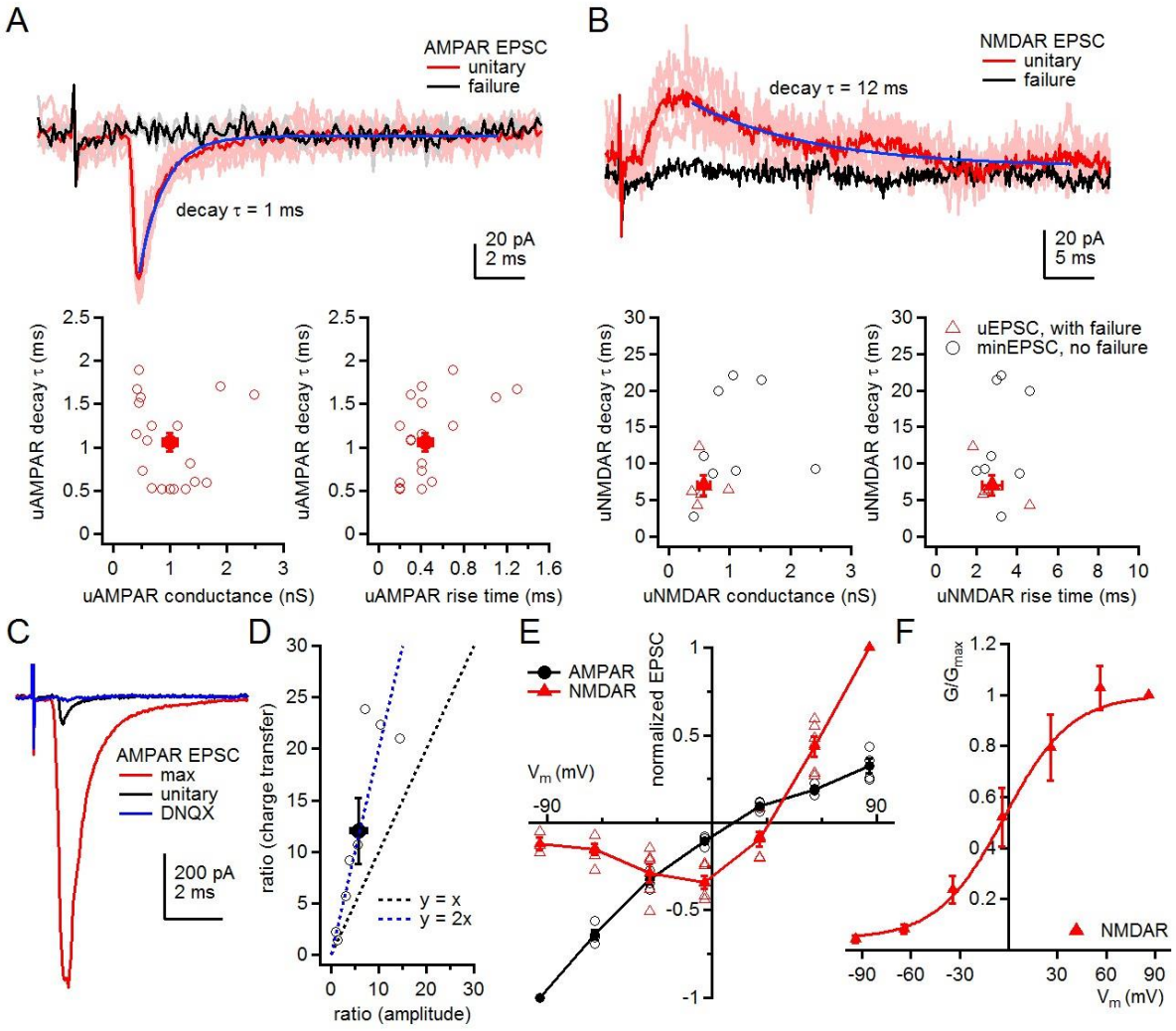

Figure 2.1. Properties of mossy fiber synaptic inputs to CbN cells.

A. AMPAR uEPSCs. *Top.* Representative traces of 10 overlaid AMPAR uEPSCs (*light red,* 8 traces) and failures (*grey*, 2 traces), with mean uEPSC (*red*) and mean failure (*black*) superimposed. *Blue* trace, exponential fit to the uEPSC decay. *Bottom*. *Left*, unitary AMPAR conductance *vs.* decay τ; *right*, unitary AMPAR 10%-90% rise time *vs.* decay τ (N=20). **B.** NMDAR uEPSCs. *Top.* Representative traces of 6 overlaid NMPAR uEPSCs (*light red*, 5 traces) and one failure (*black*), with mean uEPSC (*red*) superimposed. *Blue* trace, exponential fit to the

uEPSC decay. *Bottom. Left*, unitary NMDAR conductance *vs.* decay τ; *right*, unitary NMDAR 10%-90% rise time *vs.* decay τ (N=13). *Triangles*, responses with distinct successes and failures (N=5); *circles*, responses of similar unitary amplitude without clear failures, in which reducing stimulus intensity gave only failures (N=8). **C.** Representative traces of mean AMPAR maxEPSC, uEPSC, and response in DNQX. **D.** Convergence ratio of mossy fibers onto CbN cells estimated from AMPAR maximum response divided by unitary responses for charge transfer *vs.* current amplitude (N=8). **E.** Current-voltage relationships of AMPAR (*black*, N=4) and NMDAR EPSCs (*red*, N=6). Individual responses, *open symbols*, mean data, *closed symbols*. **F.** Voltage-dependent activation curve of NMDAR EPSG.

validate the amplitude measurements from the few unitary responses. For confirmed unitary responses, the mean NMDAR conductance was 0.57 ± 0.11 nS. The kinetics were unusually rapid for NMDARs, with rise times of 2.7 ± 0.5 ms and decay time constants of 7.0 ± 1.4 ms (N=5; 3M, 2F), resembling NMDAR kinetics measured in auditory neurons (Steinert et al., 2010).

In a subset of cells in which AMPAR uEPSCs were recorded, we also increased the stimulus intensity to evoke the largest possible AMPAR EPSC (maxEPSC), and then confirmed that the current was all AMPAR-dependent by blockade with DNQX (**Figure 2.1C**). The functional convergence of mossy fibers onto CbN cells in the slice could then be estimated by dividing the maxEPSC by the uEPSC, which ranged from 1 to 15, with a mean of 6 ± 2 (N=8, **Figure 2.1D**). Inspection of the records, however, indicated that maxEPSCs tended to be broader then uEPSCs and often contained discrete peaks (see also Mercer *et al.*, 2016), suggestive of non-concerted activation of multiple afferents or synaptic terminals. We therefore recalculated the convergence as the ratio of the charge transfer of the maximal to the unitary response. These values ranged from 1 to 22, with a mean of 12 ± 3 (**Figure 2.1D**). Thus, the data provide evidence for innervation of CbN cells by multiple mossy fibers, with an average of 12 such afferents that could be activated by electrical stimulation in the slice.

Because the voltage-dependence of EPSCs can be a distinguishing feature of different classes of glutamate receptors, we repeated recordings of pharmacologically isolated EPSCs at a range of

potentials. For these experiments, a suprathreshold stimulus intensity was used to facilitate detection of responses across the full voltage range. AMPAR EPSC amplitudes were linear up to the reversal potential, while steps above the reversal potential showed slight inward rectification of the currents (**Figure 2.1E**). Since action potentials of CbN cells rarely exceed the voltages in the linear range, we reasoned that for purposes of dynamic clamp, the currents could be treated as voltage-independent. It remains possible, however, that some fraction of the receptors are inwardly rectifying and Ca^{++}-permeable, although pilot experiments with the antagonist of Ca^{++}-permeable AMPARs philanthotoxin (10 μM) showed no consistent block of the AMPAR EPSC (N=3). NMDAR EPSCs showed a clearer voltage-dependence, although about 10% of the total conductance remained unblocked at -70 mV (**Figure 2.1E, 2.1F**), consistent with a moderate but incomplete Mg^{++} block of NMDARs of CbN cells at negative potentials (Anchisi et al., 2001; Pugh and Raman, 2006; Person and Raman, 2010).

The activity of mossy fibers *in vivo* varies in mice from a few Hz to several tens of Hz (Rancz et al., 2007; Powell et al., 2015). To assess how activity at these rates might affect synaptic amplitudes, we tested the short-term plasticity of mixed AMPAR and NMDAR EPSCs at -74 mV. The stimulus intensity was adjusted to provide initial responses of a few hundred pA, and stimulus trains were applied for 1 sec at 10, 20, 50 Hz, or for 200 ms at 90, 133, 160 Hz. (**Figure 2.2A**). Because of EPSC broadening from activation of multiple afferents and accumulation of NMDAR-mediated current with repeated stimulation, the postsynaptic current tended to summate, especially at higher stimulus rates. We therefore measured the total current relative to the pre-stimulus baseline, as a measure of how much excitatory current was flowing into the

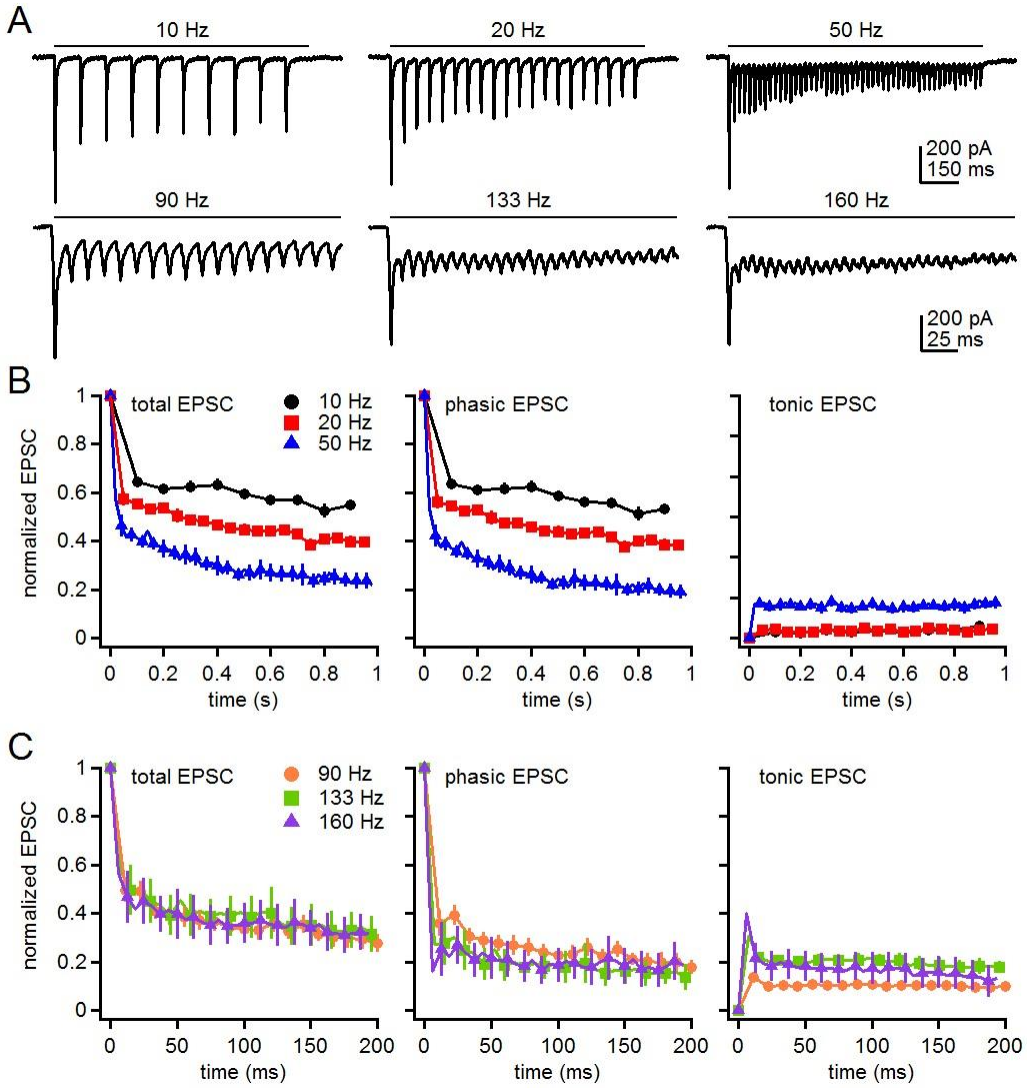

Figure 2.2. Short-term plasticity of mossy fiber EPSCs.

A. Representative EPSCs with different frequencies of electrical stimulation. All recordings are from a single CbN cell. Each trace is the mean of 5 trials. **B.** Total, phasic, and tonic EPSC amplitudes (as labeled) at low stimulus frequencies (10, 20, 50 Hz, N=8, same cells for all panels); only alternate symbols are illustrated for clarity at 50 Hz. **C.** Total, phasic, and tonic

EPSC amplitudes (as labeled) at high stimulus frequencies (90, 133, 160 Hz, N=8, same cells as in B); only alternate symbols are illustrated for clarity at 133 and 160 Hz

postsynaptic cell, but also separated the current into phasic current (the peak stimulus-evoked current measured relative to the current amplitude just before each stimulus) and tonic current (the current measured just before each stimulus). For comparison across cells, all data were normalized to the first peak EPSC (N=8; 4M, 4F; **Figure 2.2B**, **2.2C**). With progressively higher stimulation rates, total and phasic EPSCs depressed to greater extents, while tonic current began to increase. The total EPSC stabilized at 30-40% for 200 ms of stimulation at rates ≥ 50 Hz, consistent with Mercer et al. (2016). The phasic EPSCs varied from about 60% for low stimulus rates to 20% for high stimulus rates. These extents of depression were much less those that seen for climbing fiber collateral synapses onto CbN cells, which depress to 14% even when stimulated at 20 Hz and (Najac & Raman, 2016 Soc. Neurosci. Abstract), suggesting that the electrically evoked EPSCs resulted primarily from mossy fiber activation. These values of AMPAR and NMDAR EPSCs synaptic depression were later incorporated into dynamic clamp experiments.

Effects of evoked mossy fiber excitation on CbN cell firing. Before embarking on dynamic clamp experiments, we first tested how electrically evoked mossy fiber EPSPs (eEPSPs) modulate the firing of current-clamped CbN cells, as well as how this modulation is affected by concurrent inhibition. The experimental protocols were designed to be parallel to previous work (Person and Raman, 2012b), but with the addition of varying rates of excitation. $GABA_A$ receptors were pharmacologically blocked, but inhibition was applied with dynamic clamp by injecting conductances with parameters matched to Purkinje-mediated IPSCs previously measured in the same preparation (Person and Raman, 2012b). The IPSPs generated by dynamic clamp (dIPSPs)

mimicked 40 Purkinje cells each firing at 50 spikes/sec. Since simple spikes of Purkinje cells have been reported to synchronize during cerebellar behaviors (reviewed in Person & Raman, 2012b), we tested two extreme physiological possibilities by toggling the relative timing of the dIPSPs so that they either arrived asynchronously or with 20 inputs synchronized at 50 Hz while the other 20 remained asynchronous ("50% synchrony"). Thus, in all conditions, the total inhibition remained constant and only the timing of inhibition varied. Action potentials were then measured with a background of asynchronous or 50% synchronized dIPSPs, with and without stimulation of mossy fiber afferents; in every cell, these measurements were repeated for eEPSPs evoked at 90, 133, or 160 Hz, with the idea that these high frequencies would be most effective at driving CbN cells to threshold against a background of inhibition (**Figure 2.3A**, *left*).

Although CbN cells are spontaneously active at 70 to 100 spikes/s (Person and Raman, 2012b; Mercer et al., 2016), asynchronous dIPSPs were sufficient to suppress firing to rates below 10 Hz (**Figure 2.3B**, *top trace*). As expected, eEPSPs applied against asynchronous dIPSPs evoked more spikes, yielding a higher mean firing rate than in the absence of excitation (**Figure 2.3B**, *second trace*). Firing rates nevertheless remained far lower than *in vivo*, addressed in later experiments. When half the dIPSPs were synchronized, the firing rates of CbN cells increased even without excitation (**Figure 2.3B**, *third trace*), as previously reported (Person and Raman, 2012b). Interestingly, when the same rates of eEPSPs were applied with 50% synchronized dIPSPs, firing rates were elevated to values greater than those obtained against a background of asynchronous inhibition (**Figure 2.3B**, *bottom trace*, **Figure 2.3C**, N=16; 9M, 5F, 2 unknown).

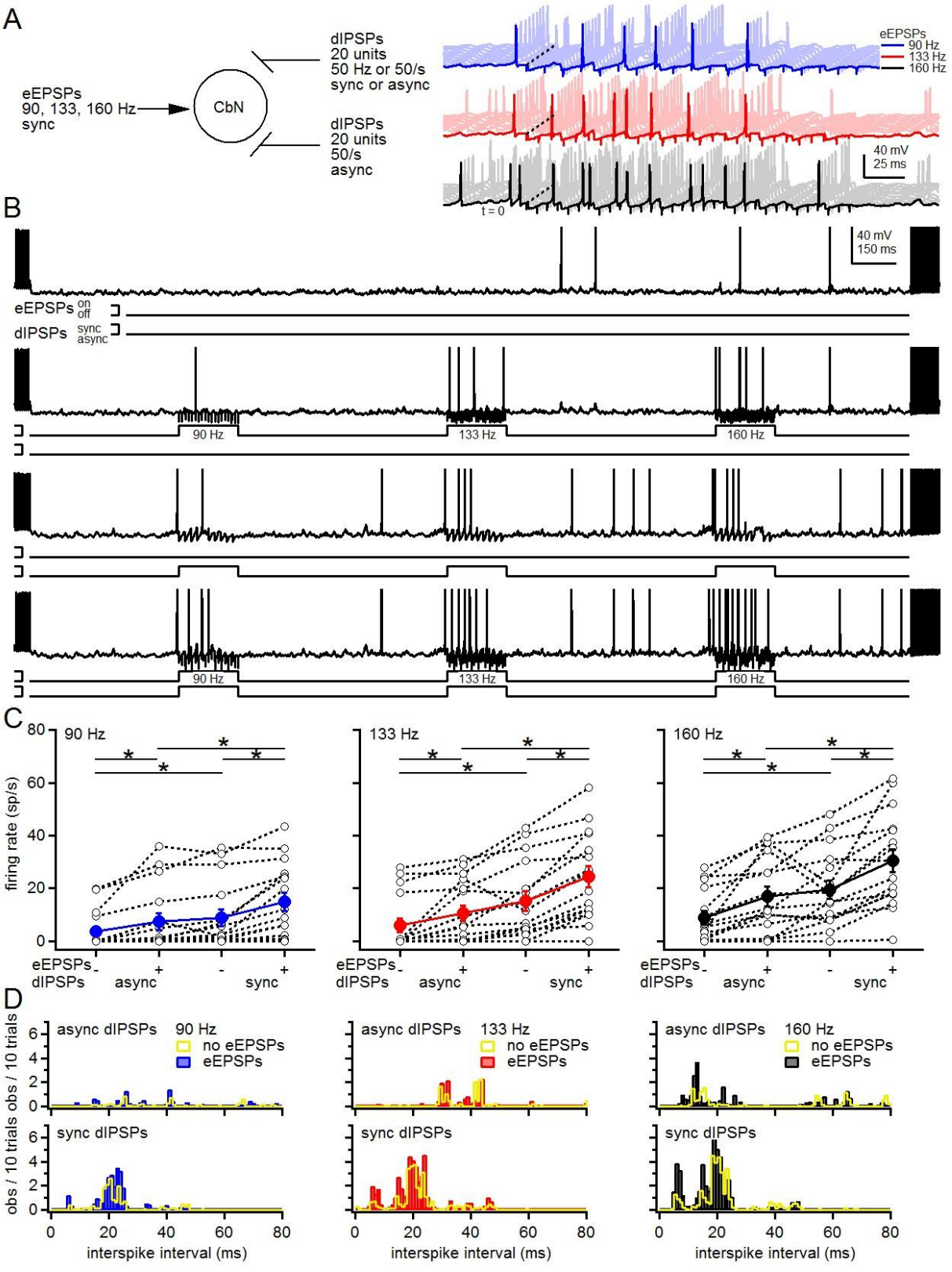
A
eEPSPs
90, 133, 160 Hz
sync
CbN
dIPSPs
20 units
50 Hz or 50/s
sync or async
dIPSPs
20 units
50/s
async
eEPSPs
90 Hz
133 Hz
160 Hz
40 mV
25 ms
t = 0
B
40 mV
150 ms
eEPSPs on off
dIPSPs sync async
90 Hz
133 Hz
160 Hz
C
90 Hz
133 Hz
160 Hz
firing rate (sp/s)
eEPSPs - + - +
dIPSPs async sync
D
async dIPSPs 90 Hz
no eEPSPs
eEPSPs
sync dIPSPs
obs / 10 trials
interspike interval (ms)

Figure 2.3. Effect of mossy fiber eEPSPs and dIPSP synchrony on CbN cell spiking.

A. *Left.* Diagram of the experimental protocol. *Right*, 10 overlaid traces with three frequencies of eEPSPs and 50% inhibitory synchrony, for comparison of spike timing across sweeps. Vertical ticks are electrical stimulation artifacts for eEPSPs (reduced for clarity). **B.** Representative traces from a single CbN cell of responses to eEPSPs and dIPSPs as labeled. In all traces, during periods of inhibition, the total amount of inhibition is constant (50/s for each of 40 units); note the slight depolarization over the course of prolonged inhibition, which raises spike probability in the second half of the interval. Upper sweeps have either asynchronous inhibition (*first* and *second* trace) or 50% synchrony applied only during the 200-ms stimulation periods (*third* and *fourth* trace). Alternate sweeps have either no excitation (*first* and *third trace*s) or eEPSPs at 90, 133, and 160 Hz applied during the stimulation periods (*second* and *fourth traces*). **C.** Firing rates of CbN cells and during the stimulation periods ± EPSPs and ± 50% synchrony, for three stimulation frequencies. *Solid symbols*, mean data; *open symbols*, individual cells (N=16, same cells, all conditions). Comparisons across conditions are made at the same time window within each sweep with repeated measures ANOVA ($p<0.01$ for each frequency), followed by paired t-tests between categories. These gave $p<0.05$ for all pairs (asterisks). **D.** Mean interspike interval histogram for all 16 cells. Observations include all intervals in 10 trials.

Since the total inhibition was constant across conditions, these data provide evidence that the degree of synchrony of IPSPs can dictate the efficacy of synaptic *excitation*. In addition to influencing the rate of spiking, the synchrony of IPSPs affected the timing of spiking. Superimposing traces indicated that when EPSPs were evoked against a 50% synchronized dIPSPs, action potentials tended to occur at fixed times that were replicable across sweeps (**Figure 2.3A**, *right*). As shown previously, without excitation, action potentials tended to phase-lock to synchronized dIPSPs, such that they occurred soon after the relief of concerted inhibition (Person and Raman, 2012b). This property is evident in the interspike-interval histograms, which show no overt pattern in the face of asynchronous dIPSPs, but cluster around 20 ms in the 50% sync condition, i.e., the interval between synchronized dIPSPs (**Figure 2.3D**, *yellow bars*). When the same measurements were made for sweeps with eEPSPs (in which excitation was necessarily synchronized owing to electrical stimulation), more spikes were elicited. The predominant intervals nevertheless remained near 20 ms, indicating that phase-locking to synchronized dIPSPs was preserved even in the presence of synchronized eEPSPs. In contrast, no systematic pattern related to the eEPSP frequency emerged for either asynchronous or 50% synchronized dIPSPs (**Figure 2.3D**, *shaded bars*). Instead, intervals with a low trial-to-trial probability during asynchronous inhibition now occurred with higher probability. The only variation was that a cluster of intervals centered at ~8 ms emerged, especially at higher eEPSP rates. We considered the possibility that these might reflect a degree of phase-locking to eEPSPs, but since 8-ms intervals were present at all eEPSP rates and even without any eEPSPs, they seem to reflect an interval between action potentials that is more likely to be intrinsically determined than a result of phase-locking to excitation.

Effects of dynamically clamped mossy fiber excitation on CbN cell firing. Although these results suggest that inhibition may regulate the rate and timing of excitation-driven action potentials in CbN cells, even the highest frequency of evoked eEPSPs applied with 50% synchrony was insufficient to elevate the firing rate much beyond 30 spikes/sec. Because this rate is well below firing rates of CbN cells in awake mice even when animals are stationary (60-90 spikes/sec, Hoebeek *et al*., 2010; Sarnaik & Raman, 2016 SfN Abstract), it seems plausible that the electrical stimulation recruits only a fraction of the total mossy fiber input, possibly because afferents are severed by slicing or because the stimulating electrode only activates a subset of existing fibers. Additionally, electrical stimulation of mossy fibers necessarily synchronizes EPSPs, which may or may not happen under physiological conditions.

Therefore, to manipulate the quantity and timing of excitatory inputs to CbN cells, we used dynamic clamp to mimic mossy fiber inputs, each with the unitary amplitude, kinetics, and voltage-dependence of the AMPAR- and NMDAR-mediated synaptic conductances that we measured. Estimates of convergence based on anatomical data were made as in Person and Raman (2012b) suggested that the number of convergent afferents might lie between 20 and 600 (detailed in *Materials and Methods*). Given that a convergence of 12 inputs could be measured in the slice, we guessed that about one-third to one-quarter of the inputs might be retained, as was the case for Purkinje afferents (Person & Raman 2012a). We therefore initially mimicked 40 convergent non-depressing mossy fiber afferents, which provided a reasonable point of departure from which more precise values could then be estimated from the experimental results (see

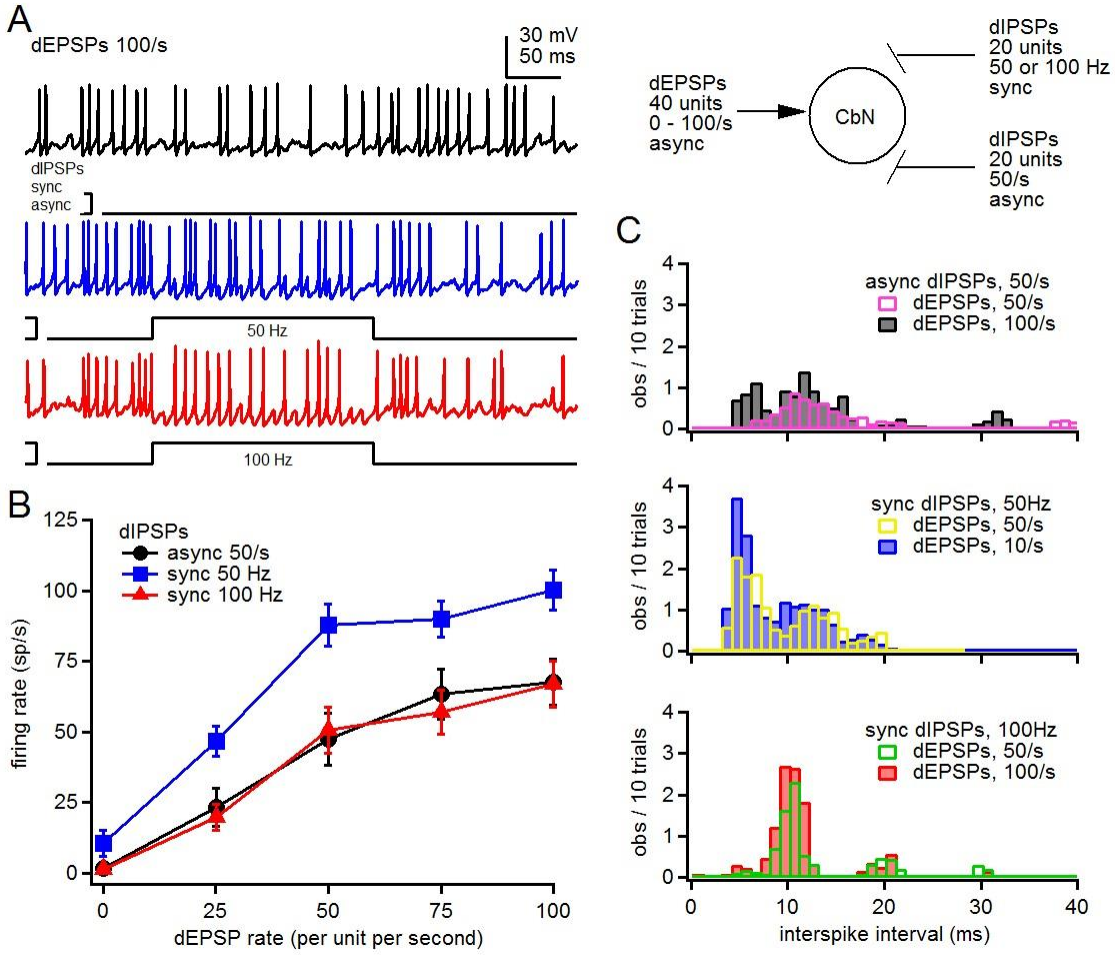

Figure 2.4. Facilitation of excitation-driven firing by inhibitory synchrony.

A. *Left,* Representative traces of CbN cell action potentials during dEPSPs, applied throughout each trace for 40 inputs each at 100/s, with dIPSPs for 40 asynchronous inputs each at 50/s throughout the trace (*black*) or switching in the marked 200-ms interval to 20 asynchronous inputs each at 50/s plus either 20 synchronous inputs at 50 Hz (*blue*) or 20 synchronous inputs at 100 Hz (*red*). *Right*, diagram of experimental protocol. **B.** Mean input-output relation in the 200-ms test intervals for CbN cell firing rates *vs.* dEPSP rate per input. Inhibition as in *A* (N=8, same cells for all conditions). Comparisons were made with a two-way repeated measures ANOVA

(*p=0.001* for synchrony, *p<0.001* for dEPSP rate; paired t-tests indicate *p<0.05* for 50% synchrony *vs.* asynchrony or *vs.* 100% synchrony for all but 0 dEPSPs. **C.** Mean interspike interval histogram for all 8 cells. Observations include all intervals in 10 trials. Data for dEPSPs at 50/s and 100/s are overlaid, as labeled.

below). Conductances were applied to evoke asynchronous dynamically clamped EPSPs (dEPSPs) at a range of rates (0 to 100/sec for each of the 40 inputs). CbN firing rates were recorded first against a background of asynchronous dIPSPs (**Figure 2.4A**, *black*). Next, inhibition was switched to 50% synchronous dIPSPs for 200 ms during each sweep (**Figure 2.4A**, *blue*). In each cell, the input-output curves for this range of excitation were measured in the 200 ms window. Importantly, total inhibition was constant while only IPSP timing varied between curves (N=8; 3M, 5F; all conditions tested in the same cells). As expected, the higher amount of mossy fiber innervation mimicked by the dynamic clamp could drive CbN cells to fire at higher rates than could be achieved with electrical stimulation of mossy fibers; these rates span the range of firing rates (excluding bursts) seen *in vivo*. Consistent with the data obtained by direct stimulation, the input-output curve was shifted to higher rates when a subset of inhibitory inputs was synchronized (**Figure 2.4B**, *black* and *blue symbols*). These results further support the idea the degree of inhibitory synchrony can gate the efficacy of excitation, for the full range of EPSP rates tested.

To explore this phenomenon further, we repeated the experiments with the rate of the synchronized inhibitory inputs raised to 100 Hz (**Figure 2.4A**, **2.4B**, *red*, same 8 cells). Despite the 50% increase in inhibition (a total of 3000 dIPSPs/sec, from 20 asynchronous inputs each at 50/sec + 20 synchronous inputs each at 100 Hz), the input-output curve overlaid that of asynchronous inhibition (a total of 2000 dIPSPs/sec, from 40 inputs each at 50/sec). These data demonstrate that neither the gain nor the linear shift of the input-output curve in response to a range of excitatory drive can be predicted by the amount of inhibition alone. Conversely, even

with known excitation, CbN firing rates cannot report the rate of inhibition. Instead, the coherence of the input from converging Purkinje cells plays a central role in defining the relationship between incoming synaptic excitation and CbN cell spikes.

Owing to the greater degree of excitation, the interspike interval histograms in the dynamic clamp experiments differed from those obtained with direct stimulation, as illustrated for 50 and 100 dEPSPs/sec per input (**Figure 2.4C**, mean of all 8 cells). With asynchronous dIPSPs, the histograms still showed a range of intervals (**Figure 2.4C**, *top*), but with 50% synchronous inhibition, instead of phase-locking with 20-ms intervals, the number of brief intervals increased since the large amount of excitation generated spike doublets and triplets (**Figure 2.4A**, *blue,* **Figure 2.4C**, *middle*). When the synchronized dIPSP rate was raised to 100 Hz, however, phase-locking was restored, evident as many 10-ms intervals and multiples thereof (**Figure 2.4C**, *bottom*). These results suggest that CbN cell spiking most effectively follows the timing patterns of coherent inhibitory inputs when the mean firing rate of CbN cells is at or below the rate of synchronized IPSPs. When the firing rate of CbN cells exceeds the rate of synchronous IPSPs, however, bursting tends to occur.

Physiological estimation of mossy fiber convergence. While this experiment illustrates qualitative aspects of the interaction between excitation and inhibition, its quantitative power was limited by two factors: First, the number of mossy fiber afferents was somewhat arbitrary, as well as at the low and of the range suggested by anatomical estimates. Second, synaptic

depression of EPSPs was not incorporated, which would have exaggerated the effect of the amount of excitation that was applied and underestimated the influence of inhibition. Additionally, a technical issue was that when the dynamic clamp imported randomized stimulation from multiple afferents, synaptic inputs that overlapped in time did not sum, introducing a small, variable error of understimulation at the highest dEPSP frequencies. Therefore, to obtain a more realistic estimate of functional mossy fiber convergence, we measured input-output curves of CbN cells with a background of asynchronous inhibition, while varying the number of injected excitatory inputs and their rates of firing. In these experiments, we also incorporated synaptic depression into the amplitudes of the injected excitatory conductances, corrected for overlapping events, and calculated the true stimulation frequencies (see *Materials and Methods*).

In the absence of excitation, asynchronous dIPSPs alone strongly suppressed firing from a spontaneous rate of 113 ± 20 Hz to 1.5 ± 1.0 Hz (N=9; 6M, 3F; **Figure 2.5A**). With 20 or 40 mossy fiber inputs, CbN cells only increased their firing slightly across the range of rates, never exceeding 35 Hz. For 80 mossy fiber inputs, firing rates of CbN cells started to approach those seen *in vivo*, ranging from just below 20 Hz to just above 80 Hz, over the range of excitation tested. (**Figure 2.5A, 2.5B**, *open symbols*, N=4; 3M, 1F). Nevertheless, given the low basal firing rates reported for mossy fibers in mice (Rancz et al., 2007; Powell et al., 2015) and the relatively high basal firing rates of CbN cells (Hoebeek et al., 2010), we reasoned that these measurements underestimated the number of mossy fibers that are likely to converge in the intact preparation. We therefore tested higher numbers of mossy fibers (200, 400, or 800). Because of

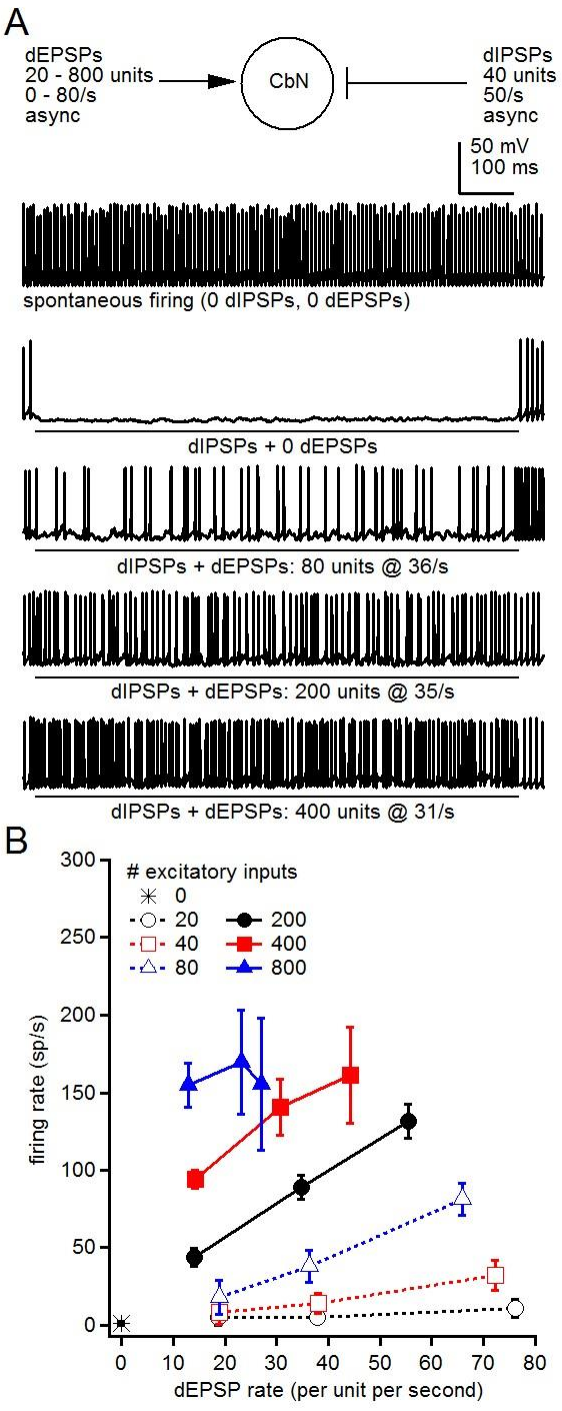

Figure 2.5. Estimation of functional mossy fiber convergence from input-output relationships.

A. *Top.* Diagram of the experimental protocol. *Bottom.* Representative traces of CbN cell firing, either spontaneously (*upper trace*), or with spontaneous firing interrupted by asynchronous dIPSPs (50/s for 40 inputs) with no excitation (*2nd trace*), asynchronous dEPSPs at 50/s for 80 units (*3rd trace*), 200 units (*4th trace*), and 400 units (*5th trace*). **B.** Input-output curves showing mean CbN cell firing rate *vs.* dEPSP rate per input for different numbers of excitatory inputs (20-80 inputs, N=4, same cells for all conditions; 200-800 inputs, N=5, same cells for all conditions, different cells than for ≤80 inputs). For 200, 400, 800 units, dEPSPs were applied as 20, 40, or 80 inputs of 10x conductance (see *Materials and Methods*).

the technical complications of injecting overlapping EPSPs, we simulated these as 20, 40, or 80 clusters of 10 simultaneous inputs (see *Materials and Methods*). For 200 inputs, CbN cell firing rates varied across the range of rates observed *in vivo* (~40-130 Hz). For 400 inputs, the firing rates of CbN cells were quite high (nearly 100 Hz even with the lowest input rate tested) and for 800 inputs, the cells fired at rates above 150 Hz across the range of inputs tested and tended to enter depolarization block. (**Figure 2.5A, 2.5B**, *closed symbols*, N=5; 3M, 2F). We therefore reasoned that conditions associated with cerebellar behaviors could be most closely mimicked by 200 active mossy fiber inputs each producing ~40 dEPSPs/sec.

Effects of jitter of synchronous inhibition. The estimate of a realistic amount of excitatory input provided the basis for testing how two key variables influence the interaction of Purkinje cell inhibition with mossy fiber excitation: (1) the fraction of convergent Purkinje cells firing in synchrony and (2) the spread or jitter on that synchrony. For these experiments, all CbN cells continuously received 200 excitatory inputs as above, each producing 40 asynchronous dEPSPs/sec to mimic a modest elevation of excitation over baseline. As before, CbN cells also received inhibition from 40 inputs, mimicking convergent Purkinje cells. Of these, 20 inputs each produced 50 dIPSPs/sec asynchronously throughout each sweep. The other 20 inputs were initially also asynchronous, at 50 dIPSPs/sec. They were then switched for a 200-ms test period, to a higher rate of 100 dIPSPs/sec, during which time the number of inputs that synchronized was varied. Five conditions were tested: synchrony of 20, 10, 4, 2, or 0 inputs, corresponding to 50%, 25%, 10%, 5%, or 0% of the total number of converging Purkinje cells. The balance of the inhibitory inputs produced asynchronous dIPSPs at 100/sec, so that the total inhibition during the

test period was consistent in all cases, schematized in **Figure 2.6A** (*diagram*). The precision of dIPSPs synchrony was also varied, so that the jitter, defined as the standard deviation about the mean event time, was 0, 0.5, 1, 2, or 4 ms.

All twenty-five conditions (5 degrees of synchrony, 5 levels of jitter) were tested in 10 cells (3M, 6F, 1 unknown). A subset of sample records is illustrated in **Figure 2.6A** (*traces*). During the test period, the firing rate of each cell varied both with the degree of synchrony and the amount of jitter. Since intrinsic firing rates varied from cell to cell, rates during the test period were normalized to the baseline rate in the pre-test period with asynchronous inhibition. For the most extreme degree of coincident inhibition tested, i.e., 20 synchronous inputs and 0 jitter, the firing rates of CbN cells during the test period were elevated to more than 2.5 times the baseline rate, even though the total amount of inhibition was constant in all conditions (**Figure 2.6B**). As the jitter increased, the firing rate was elevated to a progressively lesser extent, but remained higher than with 0% synchrony, up to a jitter of 2 ms. For 25% synchronous inhibitory inputs, the firing rates were elevated to 1.5-fold the baseline rate, and an increase in firing rate was retained up to a jitter of 1 ms. With only 10% or 5% of inhibitory inputs synchronized, CbN cell firing rates were indistinguishable from those with fully asynchronous inhibition. We repeated a subset of experiments (jitter of 0.5 ms) with a reduced shunting of the excitatory synaptic input to mimic dendritic excitation (*Materials and Methods*). Under these conditions, the extent to which the firing rate was raised again varied directly with the degree of synchrony (N=8, 4M, 4F; **Figure 2.6B**, *open symbols*). Together, these data provide the most direct and biophysically constrained evidence that, with no change in the total inhibition or excitation, as few as 10 converging

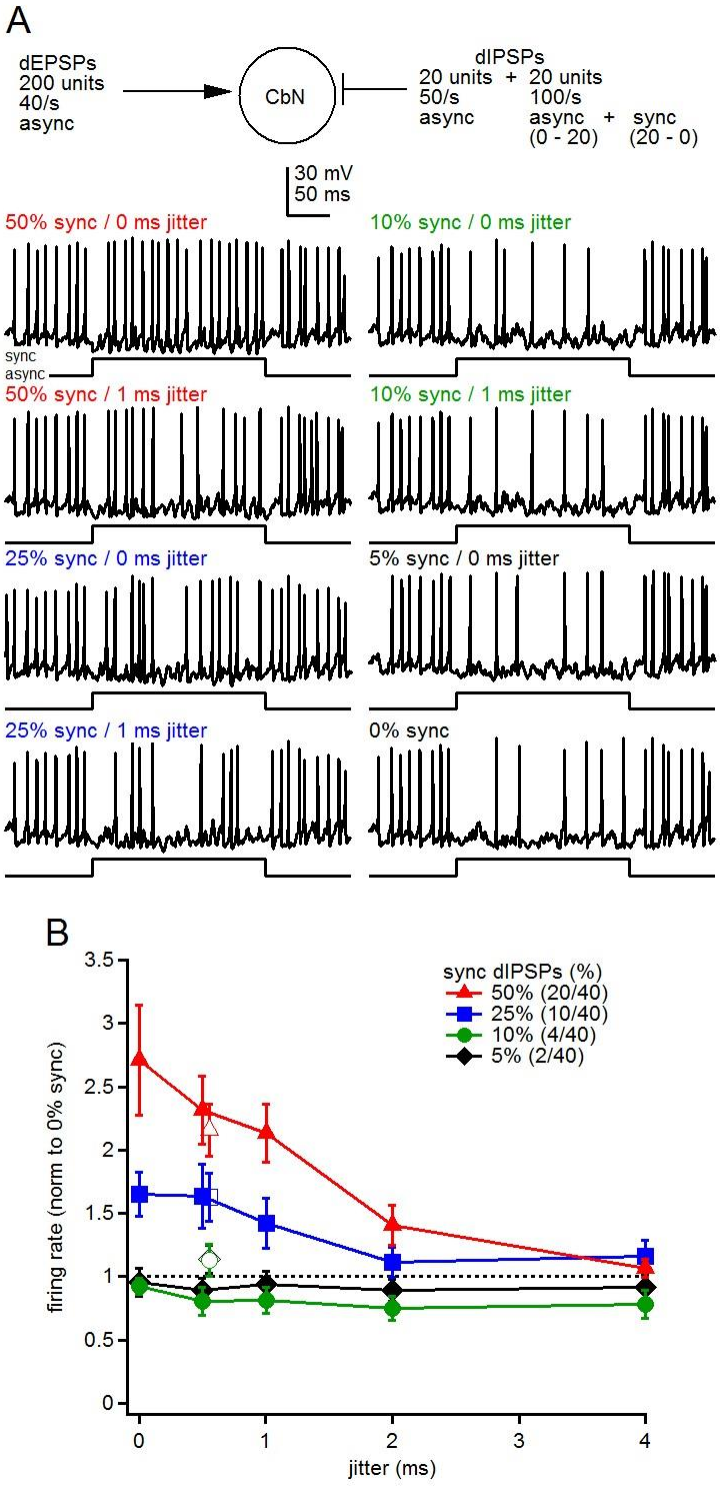
A
dEPSPs
200 units
40/s
async
CbN
dIPSPs
20 units + 20 units
50/s 100/s
async async + sync
(0 - 20) (20 - 0)
30 mV
50 ms
50% sync / 0 ms jitter
10% sync / 0 ms jitter
sync
async
50% sync / 1 ms jitter
10% sync / 1 ms jitter
25% sync / 0 ms jitter
5% sync / 0 ms jitter
25% sync / 1 ms jitter
0% sync
B
sync dIPSPs (%)
50% (20/40)
25% (10/40)
10% (4/40)
5% (2/40)
firing rate (norm to 0% sync)
jitter (ms)
0
0.5
1
1.5
2
2.5
3
3.5
0
1
2
3
4

Figure 2.6. Sensitivity of excitation-driven firing rates of CbN cells to the degree and precision of inhibitory synchrony.

A. *Top.* Diagram of the experimental protocol. *Bottom.* Representative traces for 8 of 25 conditions tested, showing CbN cell action potentials for different levels of synchrony and amounts of jitter of dIPSPs. Inhibition is initially asynchronous and switches to partly synchronous for 200-ms intervals, as labeled. Rates of excitation and inhibition are constant for all conditions. **B.** Mean firing rates of CbN cells, normalized to the rate with complete asynchrony, for different levels of inhibitory synchrony and amounts of jitter. *Solid symbols,* N=10, same cells all 20 conditions. Comparisons were made with a two-way repeated measures ANOVA ($p<0.001$ for synchrony, $p<0.001$ for jitter) followed by one-sample t-tests which gave $p<0.007$ for jitter ≤1 ms and $p>0.5$ for jitter ≥2 ms. At a jitter of 1 ms, $p=0.001$, 0.056, 0.11, and 0.58 for 50%, 25%, 10% and 5% synchrony. *Open symbols,* dEPSPs with reduced shunt to mimic dendritic excitation (N=8 additional cells; same neurons for all four conditions).

Purkinje cells firing within 2 ms of one another (i.e., with a jitter of 1 ms) can raise the firing rate of a target CbN cell by as much as 40%. In other words, the relative timing of spikes in converging Purkinje cells can control the rate of cerebellar output.

Lastly, we examined the timing of the CbN cell spikes during the test period in each condition. The interstimulus interval was binned in 1-ms increments, and the total number of spikes per bin for 10 repeated trials was measured. A subset of sample PSTHs is illustrated in **Figure 2.7A**. The restructuring of spike timing in the conditions with more synchrony and less jitter is evident as clusters of observations of spikes at particular times, interspersed with gaps. To test the degree to which the changes in spike timing were consistent across the test period, the data were collapsed across cycles for each condition, so that time 0 was the mean time of arrival of synchronized dIPSPs, and the mean number of spikes per bin following the synchronous inhibition was plotted (see *Materials and Methods*). A consistent reorganization of spike timing appeared evident for some degrees of jitter for 50% and 25% synchrony, but not for 10% or 5% synchrony (**Figure 2.7B**). With a reduced shunt of synaptic excitation, even the lower degrees of synchrony reorganized the spike timing (**Figure 2.7B**), similar to previous results with DC depolarization (Person and Raman, 2012b). To assess the temporal restructuring statistically, we performed a Rayleigh test on the unbinned spike times (see *Materials and Methods*), which reports whether the distribution of spikes within the interval following the synchronous inputs is uniform (non-significant) or non-uniform (significant). Since we had recorded ten sweeps each replicating the same combination of pseudorandom (asynchronous) and nonrandom (synchronous) stimuli in each of ten cells, we pooled the data for all ten cells but performed a separate Rayleigh test on

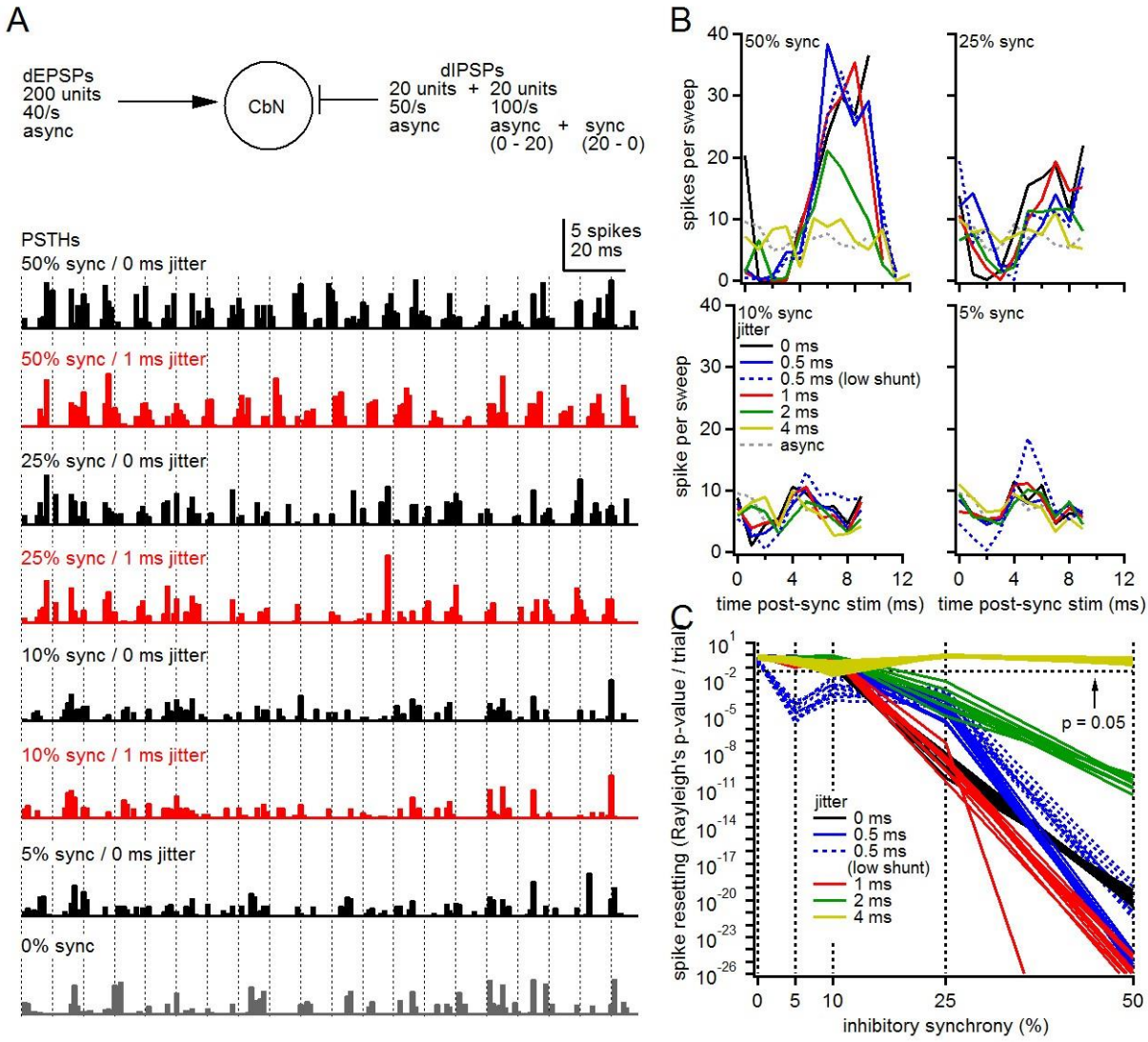

Figure 2.7. Sensitivity of excitation-driven spike timing of CbN cells to the degree and precision of inhibitory synchrony.

A. *Top.* Diagram of the experimental protocol. Same protocol and cells as in Figure 6. *Bottom.* Mean post-stimulus time histograms (PSTH, bin=1 ms, N=10) for 8 of 25 conditions tested; *dotted lines* at 10 ms intervals indicate the arrival time of synchronized dIPSPs. **B.** PSTHs (bin=1 ms) collapsed over 20 cycles of partly synchronized IPSPs and averaged across all 10 cells. *Blue*

dashed lines (“low shunt”) are from 8 additional cells with reduced shunt. The x-axis exceeds 10 ms to account for stimulus delays at high degrees of synchrony (see *Materials and Methods*). High values indicate well-timed action potentials; low values indicate effective spike suppression by inhibition. **C.** Rayleigh’s *p*-values for uniformity *vs.* level of synchrony for different degrees of jitter. Values <0.05 indicate significant resetting of spike timing in the interval following partly synchronized dIPSPs.

each trial and plotted the *p*-values; a parallel analysis was done for the eight cells with reduced shunt (**Figure 2.7C**). Under the conditions tested, synchrony of 2 or 4 inhibitory inputs was insufficient to consistently restructure CbN cell spikes significantly, regardless of the degree of jitter, unless the shunt was reduced. In contrast, for either 10 or 20 synchronous inputs, the timing of CbN cell spikes was significantly regularized by all but the maximal jitter tested. Thus, as few as 10 converging Purkinje cells firing within 4 ms of each other (i.e., with a jitter of 2 ms) can restructure the temporal pattern of CbN cell spiking. In other words, the relative timing of spikes in converging Purkinje cells can also control the timing of cerebellar output.

2.4 Discussion

The present experiments identify the properties of synaptic excitation of large CbN cells by cerebellar mossy fibers at near-physiological temperatures in weanling mice. Unitary mossy fiber inputs are relatively weak, generating mixed AMPAR and NMDAR EPSCs with small unitary conductances, fast kinetics, and moderate synaptic depression when activated at rates above 10 Hz. Consequently, the amount of excitation required for CbN cells to fire at rates reported *in vivo*, against a background of Purkinje-mediated inhibition, suggest a convergence of about 200 unitary mossy fiber inputs, or the equivalent, per CbN cell. Even when mossy-fiber driven excitation is substantial, both the rate and timing of CbN cell spikes are modulated by the degree of coincidence among Purkinje cell inputs, such that synchronizing a subset of inhibitory inputs increases firing rates and influences the time of occurrence of action potentials in CbN cells, whereas desynchronizing Purkinje inputs maximizes inhibition. The strength of this modulation varies directly with the proportion of inputs that synchronize as well as the precision, or jitter, of their synchrony. Overall, synchronizing only 25% of convergent Purkinje cells with 1 ms jitter, which corresponds to 10 inputs to a single CbN cell arriving within ~2 ms of each other, is sufficient to increase the efficacy with which mossy fibers drive spiking in CbN cells.

Characteristics of mossy fiber synapses onto CbN cells. Previous studies have shown that AMPAR EPSCs in CbN cells undergo long-term potentiation and depression (Pugh and Raman, 2006; Zhang and Linden, 2006; Person and Raman, 2010), but their unitary properties have not been quantified systematically. The unitary responses recorded here were taken to represent mossy fiber properties because the properties of synaptic depression from electrical stimulation

of multiple afferents were consistent with those of optogenetically isolated mossy fibers and not of climbing fiber collaterals (Najac & Raman 2016, Soc. Neurosci. Abstract). It cannot be ruled out, however, that some unitary responses might have resulted from climbing fiber collateral stimulation. Nevertheless, since the population of responses was relatively uniform, these values provide a reasonable first approximation until identified mossy fiber afferents can be individually activated. These unitary AMPAR and NMDAR EPSCs onto CbN cells are small, brief, and subject to mild depression. NMDAR EPSCs of CbN cells in weanling mice differ from those in <P14 slices or slice cultures from P1 rats, which are large and slowly decaying, but they share the characteristic of weak Mg^{++} block (Audinat et al., 1992; Aizenman and Linden, 2000; Anchisi et al., 2001). Along with the higher recording temperature used here, developmental changes may account for these differences. Parallel data comes from the auditory system, in which the decay kinetics of NMDAR EPSCs fall from 40-50 ms at P10 to 10-15 ms at P18 (Steinert et al., 2010), possibly owing to substitution of NR2B with NR2C during development, which also alters the Mg^{2+} block (Akazawa et al., 1994). The synaptic properties described here may also change further as mice grow into adulthood. For instance, plasticity of mossy fiber synapses is predicted during cerebellar learning (Medina and Mauk, 1999), and *in vitro* studies have shown potentiation of mossy fiber EPSCs occurs at least until P32 (Person and Raman, 2010).

Mossy fiber convergence. The present studies indicate that CbN cell firing rates comparable to those in awake behaving mice can be mimicked by 200 identical converging inputs. This value is 50 times the convergence onto cerebellar granule cells (Billings et al., 2014). This difference

may reflect the fact that information that is dispersed through granule cells, which outnumber neurons of the cerebellar nuclei by 1500:1 in mice (27 million *vs.* 18 thousand; Caddy & Biscoe, 1979), is funneled through fewer CbN cells. The convergence estimate is affected by a few assumptions, however. First, in dynamic clamp, both excitation and inhibition were mimicked as somatic conductances, which shunt one another. This approach is partly justified since Purkinje cells and mossy fibers both innervate the proximal dendrites of CbN cells; however, some mossy fiber synapses are more distal, while many Purkinje synapses are somatic (Chan-Palay, 1977; Pugh and Raman, 2006). The distal inputs might be less shunted by somatic conductances, making each unitary input stronger and leading to an overestimate of convergence; indeed, reducing the shunt of excitation with convergence held constant showed the same or stronger effects of inhibitory synchrony. Second, with no series resistance error and with a Q10 of 3, EPSC decay kinetics might be faster at 37°C. Thus, each input might actually contribute less depolarizing drive than applied here, which would underestimate the convergence ratio. A third factor is the assumption of completely asynchronous background activity of Purkinje cells. The experiments indicated that if this activity were partially coherent, the efficacy of mossy fibers would be increased, making the real convergence lower than estimated here. It is therefore worth emphasizing that the mossy fiber convergence is the equivalent of 200 active inputs under the present recording conditions but may correspond to a different anatomical number.

The heterogeneity of mossy fibers also makes it plausible that afferents from different sources have distinguishable properties. On the one hand, the dynamic range of distinct mossy fibers may be relatively homogeneous, since precerebellar neurons in the midbrain, pons, medulla, and

spinal cord, from which mossy fibers arise, share similar spontaneous firing rates and input-output relationships, measured in brain slices from mice (Kolkman et al., 2011). On the other hand, across animals *in vivo*, widely ranging mossy fiber firing rates have been reported (van Kan et al., 1993a; Gamlin and Clarke, 1995; Cheron et al., 1996; Mackie et al., 1999; Arenz et al., 2008). Additionally, mossy fibers can generate either high-frequency bursts (Eccles et al., 1971; Garwicz et al., 1998; Chadderton et al., 2004; Rancz et al., 2007; Bengtsson and Jorntell, 2009) or stationary tonic firing (Lisberger and Fuchs, 1978; van Kan et al., 1993a; Gamlin and Clarke, 1995; Arenz et al., 2008; Powell et al., 2015; Witter and De Zeeuw, 2015). Finally, distinct classes of mossy fiber synapses onto granule cells have different degrees of synaptic facilitation and depression (Chabrol et al., 2015). Therefore, factors such as firing patterns and short-term plasticity of specific classes of mossy fibers may shape the general results observed here.

The interaction of excitation with the synchrony of inhibition. The present results are biophysical, yet provide a mechanistic foundation for bridging to the physiological situation. While natural patterns of stimulation *in vivo* include variation in the firing rates of mossy fibers on multiple time scales, the parameter exploration here, i.e., varying the relative timing of inhibitory inputs against a constant barrage of excitation over a window of 200 ms, permits some general principles to be inferred. First, increasing the coherence of inhibition is likely to raise EPSP-driven firing rates across all degrees of excitation, since the phenomenon of increasing synchrony correlating with elevating spike rates is evident for spontaneous firing, mfEPSP-evoked firing, and dEPSP evoked firing regardless of the degree of shunting. Second, the

coherence of spiking by mossy fiber inputs might modulate but not override this phenomenon, since gaps in inhibition will always permit more effective excitation. In addition, although the magnitude of excitation may vary over time, the high EPSP rate (8000 per second) required to mimic physiological rates of firing here suggests that complete gaps in excitation would be rare. Third, synaptic delays in the cerebellar cortex may generate lags of a few milliseconds between direct excitation and the corresponding inhibition driven through the mossy fiber-granule cell-Purkinje pathway. Such lags may affect the onset of a response to synchronous inhibition, but the same principle will hold: for periods during which inhibitory synchrony is greater, the effect of excitation is predicted to be stronger. Conversely, given the high firing rates and convergence of Purkinje cells, even randomly occurring action potentials have a non-zero probability of overlapping and creating a short window of disinhibition afterward. Any mechanisms that actively decorrelate inhibitory inputs are likely to counteract excitation more effectively. Simply stated, CbN cells will fire more rapidly in response to more excitation, more synchrony among their inhibitory afferents, and/or less inhibitory jitter.

Consistent with the idea that disinhibiting CbN cells can drive motor behavior, optogenetically suppressing Purkinje cell firing for 50-500 ms elicits movements *in vivo* (Heiney et al., 2014a; Lee et al., 2015). On shorter time scales, cycles of concerted disinhibition can also arise from synchronized Purkinje cell firing, during which CbN cell spikes intervene between coincident IPSPs (Person and Raman, 2012b). Thus, disinhibition-related movement might occur even without complete suppression of Purkinje cell spiking, but only if sufficient depolarizing drive is present to bring cells to threshold, which was provided by direct current injection in the previous

experiments. Here, we find that even with synaptic drive held constant, synchronizing 20 inhibitory inputs more than doubled CbN cell firing rates; synchronizing just 10 inputs raised firing rates by 50%. Additionally, despite the rapid kinetics of EPSCs, the high convergence and small amplitudes of mossy fiber inputs decreases the membrane potential fluctuation resulting from synaptic excitation. Consequently, with realistic synaptic excitation, inhibitory synchrony resets spike timing as long as at least 10 converging Purkinje cells are synchronized. The coherence of Purkinje cell firing therefore creates gaps in inhibition during which mossy fibers more effectively drive cerebellar output.

An additional variable is the precision of synchrony. Most studies of simple spike synchrony report spikes from pairs of Purkinje cells occurring within 4 ms of one another (Bell and Grimm, 1969; Bell and Kawasaki, 1972; MacKay and Murphy, 1976; Ebner and Bloedel, 1981; Shin and De Schutter, 2006; Heck et al., 2007; de Solages et al., 2008; Bosman et al., 2010; Wise et al., 2010), corresponding here to 2 ms jitter (one standard deviation from the mean spike time). The present data indicate that this degree of precision can increase the rate as well as set the timing of CbN cell action potentials, as long as about 10 afferents fire together in a ~4 ms window.

This idea may provide insight into the consequences of complex spike synchrony on CbN cell firing. The temporal precision of complex spike synchrony differs from that of simple spikes; cross-correlograms of complex spikes indicate coincidence windows of tens of ms (Bell and Kawasaki, 1972; Welsh et al., 1995). Although each complex spike transmits only brief (<15 ms)

action potentials bursts along Purkinje axons (Khaliq and Raman, 2005; Monsivais et al., 2005), they can evoke prolonged inhibition (~100 ms) of CbN cell spiking, even without detectable increases in Purkinje cell firing (Blenkinsop and Lang, 2006; Bosman et al., 2010; Tang et al., 2016). Although in the flocculus, simple and complex spike synchrony can correlate (De Zeeuw et al., 1997), the present data raise the possibility that under some circumstances complex spikes might lead to phase resetting of simple spikes that increases the *asynchrony* of convergent Purkinje cells for a few hundred milliseconds, thereby increasing the efficacy of inhibition.

Regarding the central question of the transformation at Purkinje-to-CbN-cell synapses, because of CbN cells' strong propensity to fire spontaneously (Raman et al., 2000), suppression of CbN cell spikes can be achieved only by Purkinje cell activity that generates tonic inhibitory synaptic current, which pulls CbN cells away from threshold (Telgkamp & Raman 2002). Changes in such current can be achieved by changing firing rates of individual Purkinje cells and/or by changing the coherence of firing by convergent afferents. Simple spike synchrony on the time scale of milliseconds has been repeatedly reported for decades (Bell and Grimm, 1969; MacKay and Murphy, 1976; Ebner and Bloedel, 1981; Heck et al., 2007; de Solages et al., 2008; Wise et al., 2010; De Zeeuw et al., 2011) and can account for observed behaviors in cerebellar models (De Zeeuw et al., 2011). Nevertheless, it remains unknown how many Purkinje cells synchronize and for how long they do so. The current data set provides a framework for interpreting those data as they become available. Importantly, the effects seen here could be as brief as a single synchronous simple spike leading to a disinhibition response in CbN cells, or could persist for a longer time. Regardless of the time course or precision of relative synchrony, the present work

suggests that whenever Purkinje cells fire more coherently, mossy fiber inputs become more effective at increasing CbN cell firing rates. Conversely, when Purkinje cells tend toward asynchronous firing, mossy fiber excitation is more greatly counteracted. Consequently, by moving in and out of synchrony, Purkinje cells can act as a gate that permits or weakens excitatory drive.

Chapter 3: Conclusions

3.1 The functional difference between mossy fibers at granule cell synapses and CbN cell synapses

In the present study, the results suggest that mossy fiber to CbN cell EPSCs share some similarity with mossy fiber to granule cells synapses. For granule cell synapses, *in vitro* whole cell recording from P11-17 rats at room temperature showed a small but fast unitary AMPAR EPSC with 10-90% rise time of 0.2 ms and a decay time constant of ~1 ms (Silver et al., 1992); another recording from P25 rats at physiological temperature also showed a fast decay time constant of ~2 ms (Sargent et al., 2005). Similarly, our results also suggested that the AMPAR EPSC at CbN cells synapses have fast kinetics with the rise time of 0.4 ms and the decay time constant of ~1 ms. In contrast, the kinetics of the NMDAR components are quite different; the decay time constant is ~50 ms at granule cells synapses, while at CbN cells synapses it is much faster, at ~7 ms.

Functionally, CbN cells and granule cells show different synaptic responses upon stimulation of mossy fibers. Granule cells are usually silent in both *in vitro* or *in vivo* conditions, and stimulation of mossy fibers, either from direct stimulation of a single mossy fiber or from sensory input, usually evokes firing in granule cells (Chadderton et al., 2004; Rancz et al., 2007; Powell et al., 2015). The property of strong responsiveness makes granule cells an effective event detector and further transmits the signal to downstream Purkinje cells. In contrast to granule cells, CbN cells fire action potentials spontaneously at 70-100 Hz, and electrical

stimulation of mossy fiber elicits small excitatory responses in CbN cells, especially with respect to the background of ongoing non-synchronized Purkinje cells inhibition. Estimation from dynamic clamp suggests that even with the property of spontaneous firing, synaptic excitation of as many as 8000 EPSPs/s is required to counter background inhibition and maintain the basal firing of CbN cells. Considering that CbN cells and granule cell have different sizes and different membrane resistances, it is not surprising that these two types of cells respond differently to individual excitatory inputs of comparable magnitude.

The convergence ratio of mossy fibers onto CbN cells estimated by the dynamic clamp shown in the present study is ~200, which is very different from what have been estimated in granule cells (~4) (Rancz et al., 2007). Here, one rough but still noteworthy functional estimation is provided for verifying the order of magnitude of the convergence ratio. The number of granule cells and CbN cells in mice is 27 million and 18000, respectively (Caddy and Biscoe, 1979). If each mossy fiber makes contacts onto ~50 granule cells (Jakab and Hamori, 1988), 27 million granule cells at least require 0.54 million mossy fibers, based on the assumption that each granule cell receives one input. However, each granule cells may receive inputs from 4 mossy fibers (Rancz et al., 2007), leading to 2.16 million mossy fibers. Since the number of nuclear cells is 18000, on average each nuclear cell receives 120 mossy fibers if every mossy fiber makes a collateral branch. Furthermore, 18000 is the number of all nuclear cells rather than specifically glutamatergic CbN cells (Caddy and Biscoe, 1979). Since there is no evidence that every type of nuclear cell receives mossy fiber collateral projection, CbN cells may receive more than 120

mossy fibers. There are many assumptions in this estimation, but at least it shows that our estimate of ~200 mossy fibers converging onto a single CbN cell is not totally out of scale.

This difference in the convergence ratio and synaptic responses might be explained by the strategy these two systems use to process information. Information transmission from mossy fibers to granule cells is divergent, because each mossy fiber can synapse onto many granule cells; however, each granule cells can only receive input from ~4 mossy fibers (Jakab and Hamori, 1988; Rancz et al., 2007). Thus, the system that consists of granule cells with low spontaneous firing and high responsiveness may secure the external mossy fiber information to diverge to many downstream granule cells as needed and further increases the extent of impact; as the input layer of the cerebellum, this physiological strategy may amplify the input signals for further subsequent integration. Consistent with the idea, a modeling study simulating the number of mossy fibers to granule cells synapses showed that a limited rather than large number of synaptic connectivity (~4) ensures that granule cells process enough mossy fiber information, which presumably arises from different precerebellar nuclei encoding different sensorimotor information, while preventing population of granule cells from overloading. This study suggests the this divergent system has the most optimal computational power and has been evolutionary conserved (Billings et al., 2014).

In contrast, CbN cells, as the final output of the cerebellum, directly represent the final "decision" of the cerebellum. Using a convergence mechanism with each input having relatively

small “weights” may make sure CbN cells integrate enough information before altering their outputs and may increase the stability of the system. A similar strategy mighty also be found in Purkinje cells population coding: extracellular recordings from behaving monkeys showed diverse responses of individual Purkinje cell with smooth-pursuit eye movements while the population discharge could perfectly predict the movement (Dash et al., 2012). These results suggest the idea that individual Purkinje cells may receive different mossy fiber inputs each encoding different sensorimotor information, while the population of Purkinje cells represents the final integration, which has the ability to regulate CbN cells through convergence.

3.2 Synaptic plasticity might be controlled by the synchrony

The cerebellum is necessary for motor learning, and one form that has been well studied is delay eyelid conditioning (McCormick and Thompson, 1984). The animal is presented with a conditioned stimulus such as a tone and an unconditioned stimulus such as a puff of air on the eyeball; the unconditioned stimulus itself irritates the animal and causes an unconditioned response of eyelid closure. During conditioning, the animal sequentially receives a paired conditioned stimulus and unconditioned stimulus repeatedly. After pairing, the animal learns to express the unconditioned response (eyelid closure) to the conditioned stimulus (tone) (Medina et al., 2000). Experimental studies using direct stimulation of mossy fibers or the inferior olive for conditioning showed that in the cerebellar circuitry the mossy fibers carry the conditioned stimulus while the climbing fibers carry the unconditioned stimulus (Mauk et al., 1986; Kalmbach et al., 2010). Activation of CbN cells in turn drives the output responses (McCormick and Thompson, 1984).

In the circuit, before learning, the synaptic drive from the mossy fibers in response to the conditioned stimulus alone is not strong enough to activate CbN cells to drive an eyelid closure; however, after learning, mossy fibers alone can activate CbN cells. Modeling studies suggested that there may be several and not mutually exclusive possible types of modulation being induced in the circuit (Medina and Mauk, 1999). For example, intrinsic properties of CbN cells might become more excitable; Purkinje cells inhibition on CbN cells might become weaker; or synaptic drive from mossy fibers might become stronger. Many aspects of this model have been tested experimentally; some points are supported and others are still under debate. For example, the parallel fiber to Purkinje cell synapses have been proposed to induce long-term depression, which in turn weakens the Purkinje cell inhibition of CbN cells (Mauk et al., 1998; Ito, 2000); however, one study using mutant mice with a disruption of AMPA receptor internalization, which prevents depression, showed no difference in cerebellar learning behavior including delay eyelid conditioning (Schonewille et al., 2011).

One of the possibilities that is described in the model is an increase of mossy fiber drive onto CbN cells during the learning (Medina and Mauk, 1999); in the model the induction of long-term potentiation at mossy fiber synapses requires Purkinje cells inhibition of CbN cells. *In vitro* studies support the idea that Purkinje cell inhibition is necessary for induction of CbN cell potentiation (Pugh and Raman, 2006, 2008; Person and Raman, 2010). These studies demonstrated that long-term potentiation could be generated by an induction protocol containing mossy fiber excitation, CbN cell hyperpolarization by negative current injection, and rebound

burst firing of CbN cells. In this mechanism, these three steps respectively cause activation of postsynaptic calcium-dependent phosphatase calcineurin through NMDA receptors, deactivation of L-type calcium channels that prevent potentiation, and triggering of α-CaMKII by activation of voltage dependent calcium channels. Particularly, deactivation of L-type calcium channels needs hyperpolarization, which normally would be generated by Purkinje cells inhibition that is strong enough to prevent CbN cells from firing, even with mossy fiber excitation.

Physiologically, the hyperpolarization of CbN cells could be from an increase in the asynchrony of Purkinje cell simple spikes; our results suggest that an increase in the jitter of synchrony, which in turn increases the asynchrony, could also effectively hyperpolarize the cell. Generation of this asynchrony may come from the complex spike synchrony. Cross-correlation studies suggest that the complex spike synchrony has less precision than simple spike synchrony (Bell and Kawasaki, 1972; Sasaki et al., 1989; Welsh et al., 1995); it is possible that complex spike synchrony might lead to phase resetting of simple spikes that increase the asynchrony. Consistent with this idea, complex spike synchrony usually evokes prolonged inhibition of CbN cells without detectable increases in Purkinje cell firing (Bosman et al., 2010). Furthermore, the complex spike synchrony originates from co-activation of climbing fibers, which can also be considered as an unconditioned stimulus carrier. Thus, it is possible that an unconditioned stimulus might evoke complex spike synchrony, which leads to prolonged hyperpolarization of CbN cells, which in turn facilitates CbN cell potentiation.

References

Afshari FS, Ptak K, Khaliq ZM, Grieco TM, Slater NT, McCrimmon DR, Raman IM (2004) Resurgent Na currents in four classes of neurons of the cerebellum. J Neurophysiol 92:2831-2843.

Aizenman CD, Linden DJ (2000) Rapid, synaptically driven increases in the intrinsic excitability of cerebellar deep nuclear neurons. Nature Neuroscience 3:109-111.

Akazawa C, Shigemoto R, Bessho Y, Nakanishi S, Mizuno N (1994) Differential expression of five N-methyl-D-aspartate receptor subunit mRNAs in the cerebellum of developing and adult rats. The Journal of Comparative Neurology 347:150-160.

Anchisi D, Scelfo B, Tempia F (2001) Postsynaptic currents in deep cerebellar nuclei. J Neurophysiol 85:323-331.

Angelaki DE, Yakusheva TA (2009) How vestibular neurons solve the tilt/translation ambiguity. Comparison of brainstem, cerebellum, and thalamus. Annals of the New York Academy of Sciences 1164:19-28.

Arenz A, Silver RA, Schaefer AT, Margrie TW (2008) The contribution of single synapses to sensory representation in vivo. Science 321:977-980.

Armstrong DM, Edgley SA (1984a) Discharges of nucleus interpositus neurones during locomotion in the cat. The Journal of Physiology 351:411-432.

Armstrong DM, Edgley SA (1984b) Discharges of Purkinje cells in the paravermal part of the cerebellar anterior lobe during locomotion in the cat. The Journal of Physiology 352:403-424.

Audinat E, Gahwiler BH, Knopfel T (1992) Excitatory synaptic potentials in neurons of the deep nuclei in olivo-cerebellar slice cultures. Neuroscience 49:903-911.

Azim E, Fink AJ, Jessell TM (2014) Internal and External Feedback Circuits for Skilled Forelimb Movement. Cold Spring Harb Symp Quant Biol 79:81-92.

Bal T, McCormick DA (1997) Synchronized oscillations in the inferior olive are controlled by the hyperpolarization-activated cation current I(h). J Neurophysiol 77:3145-3156.

Bell CC, Grimm RJ (1969) Discharge properties of Purkinje cells recorded on single and double microelectrodes. J Neurophysiol 32:1044-1055.

Bell CC, Kawasaki T (1972) Relations among climbing fiber responses of nearby Purkinje Cells. J Neurophysiol 35:155-169.

Bengtsson F, Jorntell H (2009) Sensory transmission in cerebellar granule cells relies on similarly coded mossy fiber inputs. Proc Natl Acad Sci U S A 106:2389-2394.

Billings G, Piasini E, Lorincz A, Nusser Z, Silver RA (2014) Network structure within the cerebellar input layer enables lossless sparse encoding. Neuron 83:960-974.

Blenkinsop TA, Lang EJ (2006) Block of inferior olive gap junctional coupling decreases Purkinje cell complex spike synchrony and rhythmicity. J Neurosci 26:1739-1748.

Blenkinsop TA, Lang EJ (2011) Synaptic action of the olivocerebellar system on cerebellar nuclear spike activity. J Neurosci 31:14708-14720.

Bosco G, Poppele RE (2001) Proprioception from a spinocerebellar perspective. Physiological reviews 81:539-568.

Bosman LW, Koekkoek SK, Shapiro J, Rijken BF, Zandstra F, van der Ende B, Owens CB, Potters JW, de Gruijl JR, Ruigrok TJ, De Zeeuw CI (2010) Encoding of whisker input by cerebellar Purkinje cells. The Journal of Physiology 588:3757-3783.

Braitenberg V, Atwood RP (1958) Morphological observations on the cerebellar cortex. The Journal of Comparative Neurology 109:1-33.

Brodal P (1978) The corticopontine projection in the rhesus monkey. Origin and principles of organization. Brain 101:251-283.

Brunel N, Hakim V, Isope P, Nadal JP, Barbour B (2004) Optimal information storage and the distribution of synaptic weights: perceptron versus Purkinje cell. Neuron 43:745-757.

Caddy KW, Biscoe TJ (1979) Structural and quantitative studies on the normal C3H and Lurcher mutant mouse. Philos Trans R Soc Lond B Biol Sci 287:167-201.

Canto CB, Witter L, De Zeeuw CI (2016) Whole-Cell Properties of Cerebellar Nuclei Neurons In Vivo. PloS one 11:e0165887.

Carpenter MB, Stein BM, Peter P (1972) Primary Vestibulocerebellar Fibers in Monkey - Distribution of Fibers Arising from Distinctive Cell Groups of Vestibular Ganglia. Am J Anat 135:221-+.

Chabrol FP, Arenz A, Wiechert MT, Margrie TW, DiGregorio DA (2015) Synaptic diversity enables temporal coding of coincident multisensory inputs in single neurons. Nature Neuroscience 18:718-727.

Chadderton P, Margrie TW, Häusser M (2004) Integration of quanta in cerebellar granule cells during sensory processing. Nature 428:856-860.

Chan-Palay V (1977) Cerebellar dentate nucleus : organization, cytology and transmitters. Berlin ; New York: Springer-Verlag.

Cheron G, Escudero M, Godaux E (1996) Discharge properties of brain stem neurons projecting to the flocculus in the alert cat. I. Medical vestibular nucleus. J Neurophysiol 76:1759-1774.

Choi S, Yu E, Kim D, Urbano FJ, Makarenko V, Shin HS, Llinas RR (2010) Subthreshold membrane potential oscillations in inferior olive neurons are dynamically regulated by P/Q- and T-type calcium channels: a study in mutant mice. The Journal of Physiology 588:3031-3043.

D'Angelo E, De Zeeuw CI (2009) Timing and plasticity in the cerebellum: focus on the granular layer. Trends in Neurosciences 32:30-40.

Dash S, Catz N, Dicke PW, Thier P (2012) Encoding of smooth-pursuit eye movement initiation by a population of vermal Purkinje cells. Cerebral cortex 22:877-891.

Davie JT, Clark BA, Hausser M (2008) The origin of the complex spike in cerebellar Purkinje cells. J Neurosci 28:7599-7609.

De Gruijl JR, Hoogland TM, De Zeeuw CI (2014) Behavioral correlates of complex spike synchrony in cerebellar microzones. J Neurosci 34:8937-8947.

de Solages C, Szapiro G, Brunel N, Hakim V, Isope P, Buisseret P, Rousseau C, Barbour B, Lena C (2008) High-frequency organization and synchrony of activity in the purkinje cell layer of the cerebellum. Neuron 58:775-788.

de Zeeuw CI, Holstege JC, Ruigrok TJ, Voogd J (1990) Mesodiencephalic and cerebellar terminals terminate upon the same dendritic spines in the glomeruli of the cat and rat inferior olive: an ultrastructural study using a combination of [3H]leucine and wheat

germ agglutinin coupled horseradish peroxidase anterograde tracing. Neuroscience 34:645-655.
De Zeeuw CI, Koekkoek SK, Wylie DR, Simpson JI (1997) Association between dendritic lamellar bodies and complex spike synchrony in the olivocerebellar system. J Neurophysiol 77:1747-1758.
De Zeeuw CI, Simpson JI, Hoogenraad CC, Galjart N, Koekkoek SK, Ruigrok TJ (1998) Microcircuitry and function of the inferior olive. Trends in Neurosciences 21:391-400.
De Zeeuw CI, Hoebeek FE, Bosman LW, Schonewille M, Witter L, Koekkoek SK (2011) Spatiotemporal firing patterns in the cerebellum. Nature Reviews Neuroscience 12:327-344.
De Zeeuw CI, Chorev E, Devor A, Manor Y, Van Der Giessen RS, De Jeu MT, Hoogenraad CC, Bijman J, Ruigrok TJ, French P, Jaarsma D, Kistler WM, Meier C, Petrasch-Parwez E, Dermietzel R, Sohl G, Gueldenagel M, Willecke K, Yarom Y (2003) Deformation of network connectivity in the inferior olive of connexin 36-deficient mice is compensated by morphological and electrophysiological changes at the single neuron level. J Neurosci 23:4700-4711.
Delvendahl I, Straub I, Hallermann S (2015) Dendritic patch-clamp recordings from cerebellar granule cells demonstrate electrotonic compactness. Frontiers in Cellular Neuroscience 9:93.
Dino MR, Schuerger RJ, Liu Y, Slater NT, Mugnaini E (2000) Unipolar brush cell: a potential feedforward excitatory interneuron of the cerebellum. Neuroscience 98:625-636.
Dizon MJ, Khodakhah K (2011) The role of interneurons in shaping Purkinje cell responses in the cerebellar cortex. J Neurosci 31:10463-10473.
Ebner TJ, Bloedel JR (1981) Correlation between activity of Purkinje cells and its modification by natural peripheral stimuli. J Neurophysiol 45:948-961.
Eccles J, Llinas R, Sasaki K (1964) Excitation of Cerebellar Purkinje Cells by the Climbing Fibres. Nature 203:245-246.
Eccles JC, Rosen I, Scheid P, Taborikova H (1974) Temporal patterns of responses of interpositus neurons to peripheral afferent stimulation. J Neurophysiol 37:1424-1437.
Eccles JC, Faber DS, Murphy JT, Sabah NH, Taborikova H (1971) Afferent volleys in limb nerves influencing impulse discharges in cerebellar cortex. I. In mossy fibers and granule cells. Experimental Brain Research 13:15-35.
Gacek RR (1968) Neuroanatomical pathways of the vestibular system. Ann Otol Rhinol Laryngol 77:210-215.
Gamlin PD, Clarke RJ (1995) Single-unit activity in the primate nucleus reticularis tegmenti pontis related to vergence and ocular accommodation. J Neurophysiol 73:2115-2119.
Gao W, Dunbar RL, Chen G, Reinert KC, Oberdick J, Ebner TJ (2003) Optical imaging of long-term depression in the mouse cerebellar cortex in vivo. J Neurosci 23:1859-1866.
Gardner SM, Trussell LO, Oertel D (1999) Time course and permeation of synaptic AMPA receptors in cochlear nuclear neurons correlate with input. J Neurosci 19:8721-8729.
Garwicz M, Jorntell H, Ekerot CF (1998) Cutaneous receptive fields and topography of mossy fibres and climbing fibres projecting to cat cerebellar C3 zone. The Journal of Physiology 512 (Pt 1):277-293.
Gauck V, Jaeger D (2000) The control of rate and timing of spikes in the deep cerebellar nuclei by inhibition. J Neurosci 20:3006-3016.

Grundy D (2015) Principles and standards for reporting animal experiments in The Journal of Physiology and Experimental Physiology. The Journal of Physiology 593:2547-2549.
Gundappa-Sulur G, De Schutter E, Bower JM (1999) Ascending granule cell axon: an important component of cerebellar cortical circuitry. The Journal of Comparative Neurology 408:580-596.
Häusser M, Clark BA (1997) Tonic synaptic inhibition modulates neuronal output pattern and spatiotemporal synaptic integration. Neuron 19:665-678.
Heck DH, Thach WT, Keating JG (2007) On-beam synchrony in the cerebellum as the mechanism for the timing and coordination of movement. Proc Natl Acad Sci U S A 104:7658-7663.
Heiney SA, Kim J, Augustine GJ, Medina JF (2014a) Precise control of movement kinematics by optogenetic inhibition of Purkinje cell activity. J Neurosci 34:2321-2330.
Heiney SA, Wohl MP, Chettih SN, Ruffolo LI, Medina JF (2014b) Cerebellar-dependent expression of motor learning during eyeblink conditioning in head-fixed mice. J Neurosci 34:14845-14853.
Hoebeek FE, Witter L, Ruigrok TJ, De Zeeuw CI (2010) Differential olivo-cerebellar cortical control of rebound activity in the cerebellar nuclei. Proc Natl Acad Sci U S A 107:8410-8415.
Hoogland TM, De Gruijl JR, Witter L, Canto CB, De Zeeuw CI (2015) Role of Synchronous Activation of Cerebellar Purkinje Cell Ensembles in Multi-joint Movement Control. Curr Biol 25:1157-1165.
Husson Z, Rousseau CV, Broll I, Zeilhofer HU, Dieudonne S (2014) Differential GABAergic and glycinergic inputs of inhibitory interneurons and Purkinje cells to principal cells of the cerebellar nuclei. J Neurosci 34:9418-9431.
Isope P, Barbour B (2002) Properties of unitary granule cell-->Purkinje cell synapses in adult rat cerebellar slices. J Neurosci 22:9668-9678.
Ito M (2000) Mechanisms of motor learning in the cerebellum. Brain research 886:237-245.
Jahnsen H (1986) Electrophysiological characteristics of neurones in the guinea-pig deep cerebellar nuclei in vitro. The Journal of Physiology 372:129-147.
Jakab RL, Hamori J (1988) Quantitative morphology and synaptology of cerebellar glomeruli in the rat. Anatomy and Embryology 179:81-88.
Kalmbach BE, Ohyama T, Mauk MD (2010) Temporal patterns of inputs to cerebellum necessary and sufficient for trace eyelid conditioning. J Neurophysiol 104:627-640.
Kanichay RT, Silver RA (2008) Synaptic and cellular properties of the feedforward inhibitory circuit within the input layer of the cerebellar cortex. J Neurosci 28:8955-8967.
Kawato M, Gomi H (1992) The cerebellum and VOR/OKR learning models. Trends in Neurosciences 15:445-453.
Khaliq ZM, Raman IM (2005) Axonal propagation of simple and complex spikes in cerebellar Purkinje neurons. J Neurosci 25:454-463.
Khaliq ZM, Gouwens NW, Raman IM (2003) The contribution of resurgent sodium current to high-frequency firing in Purkinje neurons: an experimental and modeling study. J Neurosci 23:4899-4912.
Khosrovani S, Van Der Giessen RS, De Zeeuw CI, De Jeu MT (2007) In vivo mouse inferior olive neurons exhibit heterogeneous subthreshold oscillations and spiking patterns. Proc Natl Acad Sci U S A 104:15911-15916.

Kodama T, du Lac S (2016) Adaptive Acceleration of Visually Evoked Smooth Eye Movements in Mice. J Neurosci 36:6836-6849.
Kolkman KE, McElvain LE, du Lac S (2011) Diverse precerebellar neurons share similar intrinsic excitability. J Neurosci 31:16665-16674.
LeDoux MS, Hurst DC, Lorden JF (1998) Single-unit activity of cerebellar nuclear cells in the awake genetically dystonic rat. Neuroscience 86:533-545.
Lee KH, Mathews PJ, Reeves AM, Choe KY, Jami SA, Serrano RE, Otis TS (2015) Circuit mechanisms underlying motor memory formation in the cerebellum. Neuron 86:529-540.
Lefler Y, Yarom Y, Uusisaari MY (2014) Cerebellar inhibitory input to the inferior olive decreases electrical coupling and blocks subthreshold oscillations. Neuron 81:1389-1400.
Lisberger SG, Fuchs AF (1978) Role of primate flocculus during rapid behavioral modification of vestibuloocular reflex. II. Mossy fiber firing patterns during horizontal head rotation and eye movement. J Neurophysiol 41:764-777.
Llinas R, Yarom Y (1981) Properties and distribution of ionic conductances generating electroresponsiveness of mammalian inferior olivary neurones in vitro. The Journal of Physiology 315:569-584.
Llinas R, Baker R, Sotelo C (1974) Electrotonic coupling between neurons in cat inferior olive. J Neurophysiol 37:560-571.
Long MA, Deans MR, Paul DL, Connors BW (2002) Rhythmicity without synchrony in the electrically uncoupled inferior olive. J Neurosci 22:10898-10905.
MacKay WA, Murphy JT (1976) Integrative versus delay line characteristics of cerebellar cortex. The Canadian journal of neurological sciences Le journal canadien des sciences neurologiques 3:85-97.
Mackie PD, Morley JW, Rowe MJ (1999) Signalling of static and dynamic features of muscle spindle input by external cuneate neurones in the cat. The Journal of Physiology 519 Pt 2:559-569.
Mauk MD, Steinmetz JE, Thompson RF (1986) Classical conditioning using stimulation of the inferior olive as the unconditioned stimulus. Proc Natl Acad Sci U S A 83:5349-5353.
Mauk MD, Garcia KS, Medina JF, Steele PM (1998) Does cerebellar LTD mediate motor learning? Toward a resolution without a smoking gun. Neuron 20:359-362.
McCormick DA, Thompson RF (1984) Cerebellum: essential involvement in the classically conditioned eyelid response. Science 223:296-299.
McCrea RA, Bishop GA, Kitai ST (1977) Electrophysiological and horseradish peroxidase studies of precerebellar afferents to the nucleus interpositus anterior. II. Mossy fiber system. Brain research 122:215-228.
McDevitt CJ, Ebner TJ, Bloedel JR (1987) Relationships between simultaneously recorded Purkinje cells and nuclear neurons. Brain research 425:1-13.
Medina JF, Mauk MD (1999) Simulations of cerebellar motor learning: computational analysis of plasticity at the mossy fiber to deep nucleus synapse. J Neurosci 19:7140-7151.
Medina JF, Nores WL, Mauk MD (2002) Inhibition of climbing fibres is a signal for the extinction of conditioned eyelid responses. Nature 416:330-333.
Medina JF, Nores WL, Ohyama T, Mauk MD (2000) Mechanisms of cerebellar learning suggested by eyelid conditioning. Curr Opin Neurobiol 10:717-724.

Mercer AA, Palarz KJ, Tabatadze N, Woolley CS, Raman IM (2016) Sex differences in cerebellar synaptic transmission and sex-specific responses to autism-linked Gabrb3 mutations in mice. Elife 5.
Miller LE, Holdefer RN, Houk JC (2002) The role of the cerebellum in modulating voluntary limb movement commands. Arch Ital Biol 140:175-183.
Mittmann W, Häusser M (2007) Linking synaptic plasticity and spike output at excitatory and inhibitory synapses onto cerebellar Purkinje cells. J Neurosci 27:5559-5570.
Mittmann W, Koch U, Hausser M (2005) Feed-forward inhibition shapes the spike output of cerebellar Purkinje cells. The Journal of Physiology 563:369-378.
Molineux ML, McRory JE, McKay BE, Hamid J, Mehaffey WH, Rehak R, Snutch TP, Zamponi GW, Turner RW (2006) Specific T-type calcium channel isoforms are associated with distinct burst phenotypes in deep cerebellar nuclear neurons. Proc Natl Acad Sci U S A 103:5555-5560.
Monsivais P, Clark BA, Roth A, Häusser M (2005) Determinants of action potential propagation in cerebellar Purkinje cell axons. J Neurosci 25:464-472.
Mugnaini E, Sekerkova G, Martina M (2011) The unipolar brush cell: a remarkable neuron finally receiving deserved attention. Brain Res Rev 66:220-245.
Mukamel EA, Nimmerjahn A, Schnitzer MJ (2009) Automated analysis of cellular signals from large-scale calcium imaging data. Neuron 63:747-760.
Najac M, Raman IM (2015) Integration of Purkinje cell inhibition by cerebellar nucleo-olivary neurons. J Neurosci 35:544-549.
Najac M, Raman IM (2016) Synaptic excitation by climbing fiber collaterals in the deep cerebellar nuclei of juvenile and adult mice. In: 46th Annual Meeting of Society for Neuroscience. San Diego, CA, USA.
Nunzi MG, Birnstiel S, Bhattacharyya BJ, Slater NT, Mugnaini E (2001) Unipolar brush cells form a glutamatergic projection system within the mouse cerebellar cortex. The Journal of Comparative Neurology 434:329-341.
Oertel D (1983) Synaptic responses and electrical properties of cells in brain slices of the mouse anteroventral cochlear nucleus. J Neurosci 3:2043-2053.
Oertel D (1985) Use of brain slices in the study of the auditory system: spatial and temporal summation of synaptic inputs in cells in the anteroventral cochlear nucleus of the mouse. J Acoust Soc Am 78:328-333.
Onodera S (1984) Olivary projections from the mesodiencephalic structures in the cat studied by means of axonal transport of horseradish peroxidase and tritiated amino acids. The Journal of Comparative Neurology 227:37-49.
Oscarsson O (1965) Functional Organization of the Spino- and Cuneocerebellar Tracts. Physiological reviews 45:495-522.
Ozden I, Sullivan MR, Lee HM, Wang SS (2009) Reliable coding emerges from coactivation of climbing fibers in microbands of cerebellar Purkinje neurons. J Neurosci 29:10463-10473.
Person AL, Raman IM (2010) Deactivation of L-type Ca current by inhibition controls LTP at excitatory synapses in the cerebellar nuclei. Neuron 66:550-559.
Person AL, Raman IM (2012a) Synchrony and neural coding in cerebellar circuits. Front Neural Circuits 6:97.

Person AL, Raman IM (2012b) Purkinje neuron synchrony elicits time-locked spiking in the cerebellar nuclei. Nature 481:502-505.
Powell K, Mathy A, Duguid I, Häusser M (2015) Synaptic representation of locomotion in single cerebellar granule cells. Elife 4.
Prinz AA, Abbott LF, Marder E (2004) The dynamic clamp comes of age. Trends in Neurosciences 27:218-224.
Pugh JR, Raman IM (2006) Potentiation of mossy fiber EPSCs in the cerebellar nuclei by NMDA receptor activation followed by postinhibitory rebound current. Neuron 51:113-123.
Pugh JR, Raman IM (2008) Mechanisms of potentiation of mossy fiber EPSCs in the cerebellar nuclei by coincident synaptic excitation and inhibition. J Neurosci 28:10549-10560.
Raghavan RT, Lisberger SG (2017) Responses of Purkinje cells in the oculomotor vermis of monkeys during smooth pursuit eye movements and saccades: comparison with floccular complex. J Neurophysiol:jn 00209 02017.
Raman IM, Bean BP (1997) Resurgent sodium current and action potential formation in dissociated cerebellar Purkinje neurons. J Neurosci 17:4517-4526.
Raman IM, Bean BP (1999) Ionic currents underlying spontaneous action potentials in isolated cerebellar Purkinje neurons. J Neurosci 19:1663-1674.
Raman IM, Gustafson AE, Padgett D (2000) Ionic currents and spontaneous firing in neurons isolated from the cerebellar nuclei. J Neurosci 20:9004-9016.
Rancz EA, Ishikawa T, Duguid I, Chadderton P, Mahon S, Häusser M (2007) High-fidelity transmission of sensory information by single cerebellar mossy fibre boutons. Nature 450:1245-1248.
Ritzau-Jost A, Delvendahl I, Rings A, Byczkowicz N, Harada H, Shigemoto R, Hirrlinger J, Eilers J, Hallermann S (2014) Ultrafast action potentials mediate kilohertz signaling at a central synapse. Neuron 84:152-163.
Robinson FR, Fuchs AF (2001) The role of the cerebellum in voluntary eye movements. Annual review of neuroscience 24:981-1004.
Robinson HP (2008) A scriptable DSP-based system for dynamic conductance injection. J Neurosci Methods 169:271-281.
Robinson HP, Kawai N (1993) Single channel properties at the synaptic site. EXS 63:250-265.
Sargent PB, Saviane C, Nielsen TA, DiGregorio DA, Silver RA (2005) Rapid vesicular release, quantal variability, and spillover contribute to the precision and reliability of transmission at a glomerular synapse. J Neurosci 25:8173-8187.
Sarnaik R, Raman IM (2016) Firing of Purkinje cells and neurons of the cerebellar nuclei during free and optogenetically perturbed locomotion in awake mice. In: 46th Annual Meeting of Society for Neuroscience. San Diego, CA, USA.
Sasaki K, Bower JM, Llinas R (1989) Multiple Purkinje Cell Recording in Rodent Cerebellar Cortex. The European Journal of Neuroscience 1:572-586.
Schmahmann JD (1991) An emerging concept. The cerebellar contribution to higher function. Arch Neurol 48:1178-1187.
Schmolesky MT, Weber JT, De Zeeuw CI, Hansel C (2002) The making of a complex spike: ionic composition and plasticity. Annals of the New York Academy of Sciences 978:359-390.

Schniepp R, Wuehr M, Huth S, Pradhan C, Schlick C, Brandt T, Jahn K (2014) The gait disorder in downbeat nystagmus syndrome. PloS one 9:e105463.
Schonewille M, Gao Z, Boele HJ, Veloz MF, Amerika WE, Simek AA, De Jeu MT, Steinberg JP, Takamiya K, Hoebeek FE, Linden DJ, Huganir RL, De Zeeuw CI (2011) Reevaluating the role of LTD in cerebellar motor learning. Neuron 70:43-50.
Sharp AA, O'Neil MB, Abbott LF, Marder E (1993) Dynamic clamp: computer-generated conductances in real neurons. J Neurophysiol 69:992-995.
Shin SL, De Schutter E (2006) Dynamic synchronization of Purkinje cell simple spikes. J Neurophysiol 96:3485-3491.
Silver RA, Traynelis SF, Cull-Candy SG (1992) Rapid-time-course miniature and evoked excitatory currents at cerebellar synapses in situ. Nature 355:163-166.
Sims RE, Hartell NA (2005) Differences in transmission properties and susceptibility to long-term depression reveal functional specialization of ascending axon and parallel fiber synapses to Purkinje cells. J Neurosci 25:3246-3257.
Sims RE, Hartell NA (2006) Differential susceptibility to synaptic plasticity reveals a functional specialization of ascending axon and parallel fiber synapses to cerebellar Purkinje cells. J Neurosci 26:5153-5159.
Sotelo C, Llinas R, Baker R (1974) Structural study of inferior olivary nucleus of the cat: morphological correlates of electrotonic coupling. J Neurophysiol 37:541-559.
Steinert JR, Postlethwaite M, Jordan MD, Chernova T, Robinson SW, Forsythe ID (2010) NMDAR-mediated EPSCs are maintained and accelerate in time course during maturation of mouse and rat auditory brainstem in vitro. The Journal of Physiology 588:447-463.
Tang T, Suh CY, Blenkinsop TA, Lang EJ (2016) Synchrony is Key: Complex Spike Inhibition of the Deep Cerebellar Nuclei. Cerebellum 15:10-13.
Telgkamp P, Raman IM (2002) Depression of inhibitory synaptic transmission between Purkinje cells and neurons of the cerebellar nuclei. J Neurosci 22:8447-8457.
Thach WT (1968) Discharge of Purkinje and cerebellar nuclear neurons during rapidly alternating arm movements in the monkey. J Neurophysiol 31:785-797.
Thach WT (1970a) Discharge of cerebellar neurons related to two maintained postures and two prompt movements. I. Nuclear cell output. J Neurophysiol 33:527-536.
Thach WT (1970b) Discharge of cerebellar neurons related to two maintained postures and two prompt movements. II. Purkinje cell output and input. J Neurophysiol 33:537-547.
Trussell LO, Zhang S, Raman IM (1993) Desensitization of AMPA receptors upon multiquantal neurotransmitter release. Neuron 10:1185-1196.
Turecek J, Yuen GS, Han VZ, Zeng XH, Bayer KU, Welsh JP (2014) NMDA receptor activation strengthens weak electrical coupling in mammalian brain. Neuron 81:1375-1388.
Uusisaari M, Obata K, Knopfel T (2007) Morphological and electrophysiological properties of GABAergic and non-GABAergic cells in the deep cerebellar nuclei. J Neurophysiol 97:901-911.
Uusisaari MY, Knopfel T (2012) Diversity of neuronal elements and circuitry in the cerebellar nuclei. Cerebellum 11:420-421.
Van Der Giessen RS, Koekkoek SK, van Dorp S, De Gruijl JR, Cupido A, Khosrovani S, Dortland B, Wellershaus K, Degen J, Deuchars J, Fuchs EC, Monyer H, Willecke K, De

Jeu MT, De Zeeuw CI (2008) Role of olivary electrical coupling in cerebellar motor learning. Neuron 58:599-612.
van Kan PL, Gibson AR, Houk JC (1993a) Movement-related inputs to intermediate cerebellum of the monkey. J Neurophysiol 69:74-94.
van Kan PL, Houk JC, Gibson AR (1993b) Output organization of intermediate cerebellum of the monkey. J Neurophysiol 69:57-73.
Walter JT, Dizon MJ, Khodakhah K (2009) The functional equivalence of ascending and parallel fiber inputs in cerebellar computation. J Neurosci 29:8462-8473.
Welsh JP, Lang EJ, Suglhara I, Llinas R (1995) Dynamic organization of motor control within the olivocerebellar system. Nature 374:453-457.
Wilson WJ, Anderson JA, Felix D (1972) Semicircular canal input to pigeon vestibulocerebellum. Brain research 45:230-235.
Wise AK, Cerminara NL, Marple-Horvat DE, Apps R (2010) Mechanisms of synchronous activity in cerebellar Purkinje cells. The Journal of Physiology 588:2373-2390.
Witter L, De Zeeuw CI (2015) In vivo differences in inputs and spiking between neurons in lobules VI/VII of neocerebellum and lobule X of archaeocerebellum. Cerebellum 14:506-515.
Wu HS, Sugihara I, Shinoda Y (1999) Projection patterns of single mossy fibers originating from the lateral reticular nucleus in the rat cerebellar cortex and nuclei. The Journal of Comparative Neurology 411:97-118.
Wylie DR, De Zeeuw CI, Simpson JI (1995) Temporal relations of the complex spike activity of Purkinje cell pairs in the vestibulocerebellum of rabbits. J Neurosci 15:2875-2887.
Xu-Friedman MA, Regehr WG (2003) Ultrastructural contributions to desensitization at cerebellar mossy fiber to granule cell synapses. J Neurosci 23:2182-2192.
Zhang S, Trussell LO (1994a) A characterization of excitatory postsynaptic potentials in the avian nucleus magnocellularis. J Neurophysiol 72:705-718.
Zhang S, Trussell LO (1994b) Voltage clamp analysis of excitatory synaptic transmission in the avian nucleus magnocellularis. The Journal of Physiology 480 (Pt 1):123-136.
Zhang W, Linden DJ (2006) Long-term depression at the mossy fiber-deep cerebellar nucleus synapse. J Neurosci 26:6935-6944.
Zhang W, Linden DJ (2012) Calcium influx measured at single presynaptic boutons of cerebellar granule cell ascending axons and parallel fibers. Cerebellum 11:121-131.
Zhou K, Wolpert DM, De Zeeuw CI (2014) Motor systems: reaching out and grasping the molecular tools. Curr Biol 24:R269-271.